Anomalous Dynamic Behavior of Stable Nanograined Materials

by

Scott Andrew Turnage

A Dissertation Presented in Partial Fulfillment
of the Requirements for the Degree
Doctor of Philosophy

Approved October 2017 by the
Graduate Supervisory Committee:

K. N. Solanki, Chair
J. Rajagopalan
P. Peralta
K. Darling
M. Mignolet

ARIZONA STATE UNIVERSITY

December 2017

ABSTRACT

The stability of nanocrystalline microstructural features allows structural materials to be synthesized and tested in ways that have heretofore been pursued only on a limited basis, especially under dynamic loading combined with temperature effects. Thus, a recently developed, stable nanocrystalline alloy is analyzed here for quasi-static ($<10^0$ s^{-1}) and dynamic loading (10^3 to 10^4 s^{-1}) under uniaxial compression and tension at multiple temperatures ranging from 298-1073 K. After mechanical tests, microstructures are analyzed and possible deformation mechanisms are proposed. Following this, strain and strain rate history effects on mechanical behavior are analyzed using a combination of quasi-static and dynamic strain rate Bauschinger testing. The stable nanocrystalline material is found to exhibit limited flow stress increase with increasing strain rate as compared to that of both pure, coarse grained and nanocrystalline Cu. Further, the material microstructural features, which includes Ta nano-dispersions, is seen to pin dislocation at quasi-static strain rates, but the deformation becomes dominated by twin nucleation at high strain rates. These twins are pinned from further growth past nucleation by the Ta nano-dispersions. Testing of thermal and load history effects on the mechanical behavior reveals that when thermal energy is increased beyond 200 °C, an upturn in flow stress is present at strain rates below 10^4 s^{-1}. However, in this study, this simple assumption, established 50-years ago, is shown to break-down when the average grain size and microstructural length-scale is decreased and stabilized below 100nm. This divergent strain-rate behavior is attributed to a unique microstructure that alters slip-processes and their interactions with phonons; thus enabling materials response with a

constant flow-stress even at extreme conditions. Hence, the present study provides a pathway for designing and synthesizing a new-level of tough and high-energy absorbing materials.

ACKNOWLEDGMENTS

I am appreciative of financial support from the Army Research Laboratory under contract no. W911NF-15-2-0038 and the National Science Foundation under contract no. 1663287. I also gratefully acknowledge the use of facilities within the Leroy Erying Center for Solid State Science at Arizona State University and assistance with material synthesis through the Army Research Laboratory under the supervision of A. J. Roberts, M. Gallagher, and T. Luckenbaugh. I would be remiss if I did not thank my advisor, Professor Kiran Solanki, who saw more potential in me than even I saw at first and taught me how to continually develop my understanding of scientific principles. Further, I am especially grateful to my committee members, Professor Jagannathan Rajagopalan, Professor Pedro Peralta, Dr. Kristopher Darling, and Professor Marc Mignolet, many of whom were also my teachers/mentors in fascinating courses and internships, for aiding in evaluating and perfecting this doctoral research. I further wish to thank my fellow colleagues in Professor Solanki's research group who aided me in this research with helpful insight and the more than occasional helping hand. Additionally, I want to thank my parents and siblings who may not have always understood me, but loved me anyway and provided every opportunity to succeed wherever God put me. Likewise to my brilliant wife, who is responsible for providing at least some degree of everything mentioned to this point, I am especially grateful for her loving support and encouragement throughout the doctoral process. Finally, saving my greatest thankfulness for last, I thank my Lord and Savior Jesus Christ whose mercy saved me from the fate I

deserve for my shortcomings and whose grace allowed me this amazing opportunity to study, in depth, the physics of His creation.

TABLE OF CONTENTS

Page

LIST OF FIGURES

Figure Page

Figure Page

LIST OF TABLES

Table Page

1 BACKGROUND AND OBJECTIVES

The instability of nanocrystalline materials microstructural features, such as grain size, has plagued development of a scientific understanding of the effects of nanocrystalline grain size on the flow stress and ductility of a material that maintains nanocrystalline structure. Without such an understanding, nanocrystalline materials will be limited to nonstructural applications despite the potential for nanocrystalline grain material to increase the load bearing potential without adding weight to the structure. Recent developments, however, have improved nanocrystalline stability in Cu using additions of an immiscible Ta solute which provides grain size stability up to temperatures of 600 °C [1]. However, only limited characterization of the alloy has been performed leaving many unanswered questions, such as the coupling of strain rates with high temperatures, the stability of the flow stress response with respect to very high strain rates (up to 10^5 s^{-1}), and the tensile response of the material. Therefore, using this alloy system, the effects of nanocrystalline microstructure on the mechanical behavior of a nanocrystalline (NC) Cu-Ta alloy will be investigated under extreme environments such as high temperature and high strain rate loading. Further, pre- and post-deformation microstructures will be analyzed to determine the deformation mechanisms present when grain rotation and growth are not allowed as well as the varied effects of Ta concentration and extrusion temperature on the mechanical behavior of these alloys.

1.1 Nanocrystalline Materials

The flow stress of a material is known to be primarily dependent on the microstructure of the material. Microstructural defects such as grain boundaries, twin boundaries, and precipitates have been shown to cause strengthening in crystalline materials. Particularly, the Hall-Petch relationship [2] defines the interaction between flow stress and grain size for a majority of crystalline solids where, as grain size reduces, flow stress increases. For this purpose, nanocrystalline materials, with grain size less than 100 nm, are an attractive prospect for structural applications where weight is a major concern. Generally speaking, as the flow stress of a material increases, the ductility of that material will decrease as the increased energy required to plastically deform the material comes from obstacles to dislocation motion which facilitates ductility. However, in the case of nanocrystalline materials such as Ni-Al and Cu alloys, a change in deformation mechanism from dislocation nucleation, propagation, and absorption to grain rotation and coalescence causes the material to exhibit superplastic behavior exhibiting strains of several hundred percent [3,4]. This makes nanocrystalline materials attractive for the purpose of energy absorbing applications such as armor plating and vehicle structures. However, nanocrystalline materials are plagued by problems relating to stability of the nanostructure; namely, under harsh environmental conditions (e.g., high temperature and complex loading states), nanocrystalline materials can undergo extensive grain growth causing the material to become microcrystalline, thereby, losing all beneficial properties from the nanocrystalline structure.

The thermal stability of NC Ni (10-20 nm) was investigated by Klement et al. [5] who measured the grain growth of NC Ni using digital scanning calorimetry and found that Ni nanocrystals became unstable and experienced significant growth at around 353 K. Further, a number of review works have been published that discuss the stabilizing mechanisms within nanocrystalline materials [6–9]. These works report that high purity nanocrystalline materials exhibit extensive instability at low homologous temperatures, but stabilization can be achieved with the introduction of stabilizing elements. While thermal stability is a major problem for nanocrystalline materials in a number of applications, the larger problem for nanocrystalline materials at low temperature applications is the instability of the structure under complex load conditions.

The mechanical stability of nanocrystalline materials poses a problem with regard to use in structural applications especially where loading states can be very complicated. Padilla and Boyce [10] composed a review of the behavior of nanocrystalline materials under fatigue loading pointing out that while nanocrystalline materials have potential to exhibit exceptional fatigue resistance, the instability of the structure promotes grain growth followed by crack formation. Further, high speed shear testing of copper, brass, and aluminum materials processed by severe plastic deformation showed extensive microstructural change as a result of high speed shear [11]. Such microstructural changes can result in deterioration of mechanical properties of a structural material under in service loading conditions. However, recent efforts have shown that nanocrystalline alloys can be stabilized to maintain nanocrystalline structure up to temperatures of 600 °C and strain rates on the order of 10^3 s^{-1} [1,12]. Stabilizing mechanisms for

nanocrystalline materials such as kinetic and thermodynamic mechanisms have been proposed and shown to be effective, but according to the work of Koch et al. [9], kinetic mechanisms, i.e., Zener pinning, are more effective at pinning nanocrystalline grain boundaries at higher homologous temperatures. This work will utilize an alloy, NC-Cu-10at.%Ta, with Ta additions that pin grain boundaries such that the nanocrystalline structure remains stable up to 400 °C [13] in order to investigate the dynamic behavior of a stable, nanocrystalline alloy.

1.2 Flow Stress-Strain Rate Sensitivity

Before the dynamic behavior of a material can be discussed, a basic understanding of strain rate sensitivity in materials is required. Using OFHC Cu as a model material for this discussion, Figure 1.1 shows that flow stress response with respect to strain rate can be divided into three distinct regions: 1) a thermal activation region where deformation is dominated by thermally activated mechanisms such as dislocation slip and twin formation, 2) a transition region which is dependent on many factors including material microstructure and lattice properties, and 3) an upturn region, here called the phonon drag region, which is classically stated to be resultant from drag forces due to mobile lattice dislocation interactions with lattice vibrations (i.e., phonons). Experimental data in Figure 1.1 comes from Jordan et al. [14] and House et al. [15].

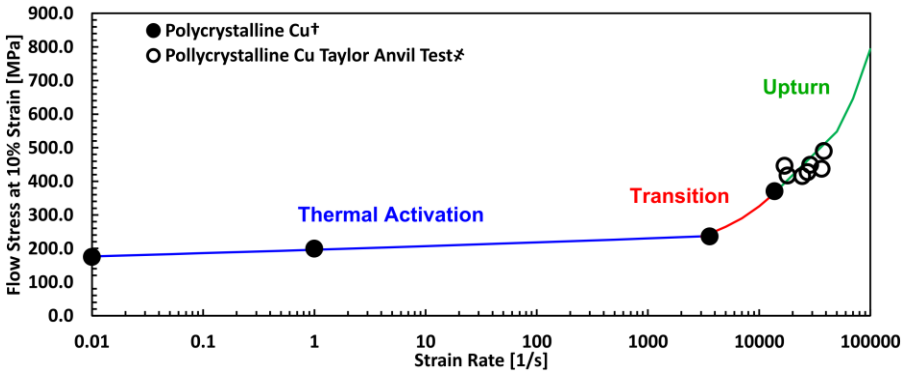

Figure 1.1 Flow stress as a function of strain rate for OFHC Cu. Experimental results come from works by Jordan et al. [14] (†) and House et al. [15] (≠). The thermal activation, transition, and upturn regions are marked with blue, red, and green lines, respectively.

The thermal activation region occurs at low strain rates, typically below 10^3 s^{-1}, where the energy required to deform the sample is determined by the activation energies of the barriers to dislocation motion within the sample (e.g., grain boundaries, precipitates, twin boundaries, etc.). The effect of energy barriers can be schematically seen in Figure 1.2 taken from [16]. As the energy input into a system increases, barriers in the system are more easily overcome leading to plastic deformation. When the energy input into the system increases sufficiently, other mechanisms may be activated though they may not be the energetically more favorable mechanism. In the case of high strain rate loading, this occurs when the usually energetically favorable mechanism of dislocation motion does not have sufficient time to occur, so energy builds to allow other mechanisms, e.g., twinning, to become dominant. As an example, this is seen to occur in OFHC Cu where high strain rate conditions can produce a nanotwinned microstructure [17].

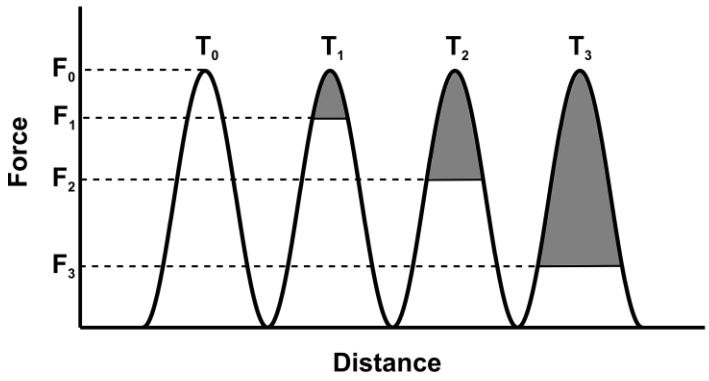

Figure 1.2 Schematic for visualizing energy barriers. As temperature increases, ($T_0 < T_1 < T_2 < T_3$), the mechanical force required to overcome a barrier is decreased. Image is adapted from [2].

The upturn in flow stress at strain rates generally higher than 10^3 s^{-1} is common to many materials, but the transition from thermal activation to phonon drag differs for each material. The transition to the flow stress upturn is dependent on many factors only some of which have been identified. Most notably for this work, the dependence of flow stress upturn on the grain size of the material is clearly observed in Ni in the work by Dalla Torre et al. [18] which is summarized in Figure 1.3. Here, it can be seen that as grain size is reduced, the upturn in flow stress exhibits an increase in flow stress at lower strain rates than that seen in coarse grained Ni. However, pure NC Ni is known to exhibit localized grain growth at high strain rates [18], so in order to understand the specific effects of factors such as grain size on the transition to the phonon drag region, the mechanisms controlling the upturn must be understood.

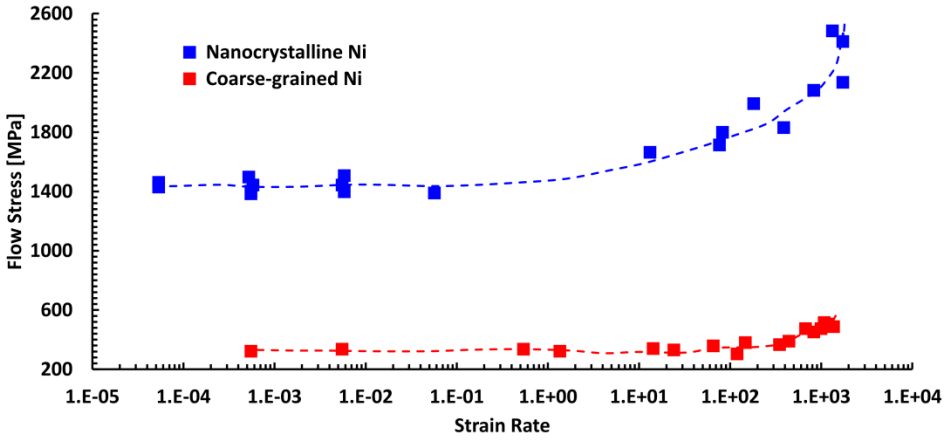

Figure 1.3 Flow stress upturn as a function of strain rate for Ni of both coarse grained and nanocrystalline grain size. Data is replotted from Dalla Torre et al. [18].

The classical understanding of the mechanism driving the upturn in flow stress is that of dislocation drag [19]. When material deformation is dominated by dislocation drag, the model for drag force on the dislocation is simply

$$F = Bv \tag{1.1}$$

where v is the average dislocation velocity and B is a drag constant as determined by

$$B = B_e + B_{ph} + B_m \tag{1.2}$$

where B_e is electron drag which is only active at temperatures below the Debye temperature (typically less than ambient temperatures), B_m is magnon drag which only comes into play for magnetic or neo-magnetic materials, and B_{ph} is phonon drag which has a greater impact at high temperatures and high strain rates as phonon drag is caused by interactions between fast moving dislocations and vibrating lattice atoms [20].

In general, we know that the classical quantum mechanical description predicts the nature of phonons to obey Bose-Einstein statistics [21]; hence, the mean occupancy number of phonons increases linearly with temperature. As the number of phonons increases, drag force on a mobile dislocation also increases leading to a rapid increase in flow stress at low strain rates. In principle, crystalline-defects (twin boundaries and/or dislocations) at elevated temperatures are free to move within the microstructure and will interact with a viscous phonon gas (derived from random lattice vibrations) leading to an increase in the drag effect during high-rate deformation. Additionally, the result of accelerating defect dislocations (full and twin) to dynamic rates is known to produce elastic waves in the form of anharmonic radiation, with a wavelength that is dependent on and proportional to the velocity [22]. However, at finite temperatures, the emitted phonons from dislocations or other sources will be partially absorbed or scattered by the viscous medium of thermal phonons and likely not travel extended distances. A high density of barriers, such as grain/twin boundaries and a high number density (6.5×10^{23} m^{-3}) of nanoclusters can lead to scattering, absorption, and transmission, which should distort the local phonon density of states and produce perturbations in the elastic/plastic front. Such interfaces/defects are known to significantly influence thermal transport properties [23].

Recently, some atomistic studies showed that decreasing grain sizes in pure NC metals enhances both the low and high frequency phonon density of states (DOS) [14,22,24]. These works showed that the lower atomic density in grain boundary regions enhances the low-frequency vibrational modes as well as promotes general broadening of

the phonon DOS due to disorder; whereas, the internal stresses within the NC grains shift the phonon DOS to higher frequency [24]. Alternatively, and in addition to contributing to the scattering and absorption of phonons, boundaries and nanoclusters can delay the transition to the drag regime by acting as barriers that pin and slow down defect propagation.

Beyond the scattering of phonons, the average dislocation velocity also plays a very important role in the effects of phonon drag on the flow stress of the material. Particularly, when a dislocation travels through a lattice with no dislocation barriers, the drag force on the dislocation limits the dislocation to travel at a maximum velocity. However, when the dislocation motion is interrupted by a barrier such as a grain boundary or precipitate, the dislocation velocity can be slowed below the critical velocity at which phonon drag becomes relevant. The average dislocation velocity is measured as the average distance between barriers divided by the time for the dislocation to both become free from the barrier ($\Delta t_{barrier}$) and travel across the open lattice (Δt_{ph}) as in

$$v_{disl} = \frac{L}{\Delta t_{barrier} + \Delta t_{ph}} \tag{1.3}$$

where

$$\Delta t_{barrier} = \Delta t_0 exp\left(\frac{(\tau_{max} - \tau)V}{kT}\right) \tag{1.4}$$

$$\Delta t_{ph} = L\sqrt{\left(\frac{B}{\tau b}\right)^2 + \left(\frac{1}{c_t}\right)^2} \tag{1.5}$$

L is the average length between barriers to dislocation motion, Δt_0 is an adjustable parameter indicating the time for a single attempt for the dislocation to depin from the first barrier, τ_{max} and τ are the maximum and applied critical shear stresses, respectively, V is the activation volume, k is Boltzmann's constant, T is the temperature, B is the drag coefficient, b is the Burger's vector of the lattice, and c_t is the approximate transverse wave speed of the lattice [25]. According to these results combined with equation 1.1, if the distance between dislocation barriers is sufficiently small, the time spent by the dislocation travelling through the lattice will be reduced such that effects of phonon drag will be minimized. This provides the basis for investigating the dynamic mechanical behavior of a material that maintains nanocrystalline structure.

1.3 High Strain Rate Testing Technique Overview

Determination of flow stress at a range of strain rates from 10^{-3} to 10^{5} s^{-1} will require multiple testing techniques including an electromechanical universal testing machine, a Kolsky bar (sometimes called a split Hopkinson pressure bar), and a rigid Taylor anvil test. Specifics of the employed techniques will be discussed in further detail throughout the work, but some theory and prior developments regarding the Kolsky bar and Taylor test will be discussed here.

The Kolsky bar technique has been well established and several good reviews of the technique have been published [26,27]. This device, outlined in Figure 1.4, employs a

system of three bars intended to deform elastically. The first bar (striker bar) is propelled by a compressed nitrogen powered gas gun toward the end of the second bar (incident bar). The strain pulse generated from the impact travels down the incident bar to the specimen where the strain wave splits into a transmitted wave and a reflected wave. Waves trapped reflecting within the specimen are deemed negligible with respect to the incident and transmitted waves.

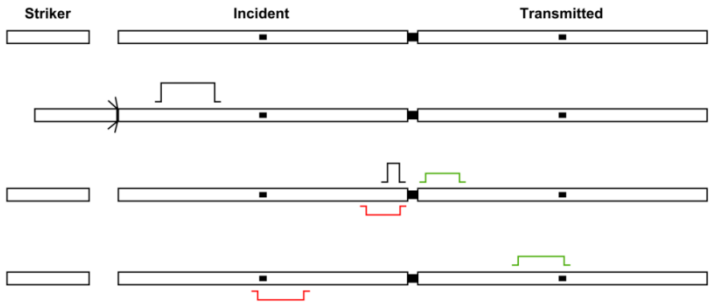

Figure 1.4 Schematic showing wave propagation through a Kolsky bar. The black, red, and green waves are the incident, reflected, and transmitted waves, respectively.

The transmitted wave travels from the specimen into the third bar (transmitted bar) where a strain gauge measures the magnitude and duration of the wave which give the engineering stress measured in the specimen as

$$\sigma = \frac{\varepsilon_T E A_b}{A_s} \tag{1.6}$$

where ε_T is the strain measured in the transmitted bar, E and A_b are the Young's modulus and cross-sectional area of the transmitted bar, respectively, and A_s is the cross-sectional area of the specimen. Similarly, the strain in the specimen can be found using the reflected strain pulse (ε_R) as

$$\varepsilon = \frac{2c_0}{l_s}\int_{t_1}^{t_2} \varepsilon_R(t)dt \tag{1.7}$$

where c_0 is the longitudinal wavespeed in the bar, l_s is the sample length, and t_1 and t_2 are the times at the start and end of the reflected pulse, respectively. As a result of the short deformation time during Kolsky bar testing, force equilibrium on each side of the specimen is not attained until plastic deformation has already begun. Further, at high strain rates and high strain levels, adiabatic heating causes softening in samples as mechanical energy is converted to thermal energy which cannot escape the specimen within the short time of deformation, so flow stress should be determined at low levels of strain but not so low that force equilibrium is not achieved, see Figure 2.2. In this work, samples of 3 mm gauge length were determined to achieve force equilibrium shortly before 10% strain, so this is the strain level at which flow stress comparisons will be made. Also, the rise in temperature resulting from adiabatic heating is calculated according to the method of Kapoor and Nemat-Nasser [28].

A full investigation of the stability of the investigated NC material requires the use of high temperatures during mechanical load application. This presents unique problems in Kolsky bar testing as the results are dependent on the elastic properties of the loading rods which will change with temperature. However, in this work Inconel 718 was used as the bar material to minimize the effects of temperature, and correction for the remaining thermal gradient has been applied using the work of Bacon et al. [29] in the form

$$\varepsilon = \frac{4c_T E(\varepsilon_i - \varepsilon_t)}{(E_T + \sqrt{E * E_T})l_s} \tag{1.8}$$

$$\sigma = \frac{\varepsilon_t E_T A_b}{A_s} \tag{1.9}$$

where ε and σ are the strain and stress in the sample, respectively, c_T is the wavespeed in the bar at the testing temperature, E and E_T are the elastic moduli at room temperature and testing temperature, respectively, ε_i and ε_t are the strain measured in the incident bar and transmitted bars, respectively, l_s is the sample length, and A_s and A_b are the cross-sectional areas of the sample and bar, respectively.

The Kolsky bar is limited to strain rates between 10^3 and 10^4 s^{-1}, so in order to evaluate mechanical behavior above 10^4 s^{-1}, a rigid Taylor anvil test capable of obtaining strain rates on the order of 10^5 s^{-1} is conducted by directly firing a cylinder of the material using a compressed gas gun at a maraging steel, rigid target plate. The test was first explained by Taylor [30] who, assuming linear deceleration, used the initial specimen length, post deformed specimen length, and velocity of the projectile to approximate the yield stress of the material. Jones et al. [31] and House et al. [15] later developed Taylor's analysis to lead to the following formulation which accounts for nonlinear deceleration

$$\sigma_y = \frac{\rho f v_s [l_0(l_1 - X)]}{(l_0 - X)(l_0 - l_1)} \tag{1.10}$$

where ρ and v_s are the density and velocity of the projectile, respectively, f is a fitting factor from 0 to 1 where ½ corresponds to Taylor's linear deceleration assumption, l_1 and

l_0 are the deformed and initial specimen lengths, respectively, and X is the undeformed section length at the end of impact [16]. This approximation was used by House et al. [15] on a number of samples including OFE Cu (f = 0.64), so it will be used in this work as a reasonable approximation of the yield stress. The average strain rate of deformation is estimated by

$$\dot{\varepsilon} = \frac{v_s}{2l_d} \tag{1.11}$$

where l_d is the length of the deformed section of the sample [30]. This approximation, developed by Taylor, assumes uniform deceleration.

1.4 Objective of the Dissertation

The objective of this research is to determine the effects of stable, nanocrystalline grain structure on the mechanical properties of a material under extreme mechanical and thermal loads. To accomplish this, the following tasks must be completed:

1. Quantify the mechanical behavior of a stable, NC-Cu-10at.%Ta alloy under uniaxial compression and tension at quasi-static and high strain rates as well as elevated temperatures.
    a. Quasi-static and dynamic tests will be employed at temperatures ranging from 298 to 1073 K and strain rates from 10^{-3} to 10^{5} s^{-1} in order to measure the stability of the flow stress.

b. Ductility of the NC alloy will be measured during tensile tests to determine whether or not the material experiences superplasticity as observed in NC pure Cu.

2. Characterize the microstructure of the alloy both before and after deformation and correlate the microstructure of the alloy with its unique dynamic mechanical behavior.
    a. As the mechanical behavior of any alloy is dependent on the structure of that material, the evolution of the nanostructure will be characterized with transmission electron microscopy (TEM) post deformation to determine what deformation mechanism is prevalent.
    b. Material with different Ta concentrations processed at differing temperatures will be analyzed to determine which structural features (e.g., grain size and Ta nano-dispersions) affect the mechanical behavior of the material system.
3. Develop and validate novel testing techniques to measure the dynamic Bauschinger effect of metallic samples.
    a. Modify a Kolsky bar to apply tension and compression pulses on opposing ends of the bar and determine a method for applying equal strain rates at a controllable delay time
    b. Validate the Kolsky bar modifications and test methodology by performing tension followed by compression and compression followed

by tension tests on 6061-T6 aluminum alloy both with and without a delay between forward and reversed loading

4. Quantify the dynamic Bauschinger effect for NC-Cu-10at.%Ta.
    a. Using a similar setup to objective 3, apply compression followed immediately by tension to a NC-Cu-10at.%Ta sample and compare to quasi-static and high strain rate results obtained separately in compression and tension

2 BREAKDOWN OF SUPERPLASTIC BEHAVIOR IN NANOCRYSTALLINE ALLOYS

The superplastic flow in structural materials is universally believed to be enhanced as the average grain size is decreased, i.e., materials with an average grain size below 100 nm can be expected to exhibit superplastic behavior at room temperature, as compared to above 50% of homologous temperature for coarse grained materials. Here we show, via systematic experiments and through computation that superplastic behavior in a truly stable nanocrystalline (NC) material is unattainable. The mechanisms driving this unexpected trend are interactions of grain boundary regions with nano-clusters, leading to a reversal or elimination of grain boundary sliding and rotation, even near the melting point of the alloy. We further present that the NC alloy studied here, exhibits a *limited* rate of strain hardening i.e. a mechanically elastic perfectly plastic response along with minimal texture changes (i.e., minimum grain size, morphology and orientation changes). Finally, deviations in superplastic behavior from the well-established notion, leads to a strong enhancement of high temperature properties, i.e., high temperature strength is remarkably maintained up to temperatures as high as 80% of the melting point (~1356 K). Thus, our results show that stabilizing the grain boundaries, by interactions with nano-clusters, can be a valuable design tool for developing advanced materials for various broad applications including the transportation and energy sectors as well as for shielding and protection applications.

The universally accepted theoretical framework suggests that within the experimental limits, a material can undergo extensive deformation, well beyond its usual breaking

point, to the extent of several hundreds of percent strain without undergoing failure if the grain size is reduced to a nanometer range. However, in this paper, contrary to the conventional belief and hitherto, we discover that a truly stabilized nanocrystalline material will not exhibit superplastic behavior even when subjected to temperature as high as 80% of its melting point. Thus, by suppressing the grain growth processes, the paper highlights a unique materials design principle through which materials with extraordinary strength and high temperature stability can be developed for advanced applications.

2.1 Introduction

Structural superplasticity is a state in which a crystalline material can undergo extensive deformation, well beyond its usual breaking point, to the extent of several hundreds of percent strain without undergoing failure. As a prerequisite, these materials must exhibit a strain rate sensitivity parameter ($m = d(\ln \sigma)/d(\ln \dot{\varepsilon})$) greater than 0.3 under controlled strain rates, usually between 10^{-4} and 10^{-2} strain-per-second, while exhibiting a *limited* rate of strain hardening i.e. a mechanically elastic perfectly plastic response along with minimal texture changes [32]. For instance, under ambient conditions, coarse grained (CG) metals and alloys generally exhibit low strain rate sensitivities, i.e., m values of less than 0.01. However, in face centered cubic (FCC) metals such as copper, as the homologous temperature is increased and or the grain size reduced, the magnitude of m parameter can approach 1, i.e., the metal will deform as a Newtonian viscous solid. Such a state, i.e., superplasticity, is usually achieved during inelastic loading at high homologous temperatures (typically $T/T_M > 0.5$ where T_M is the

absolute melting point) in a material having a fine grain size (typically less than 10 μm in diameter) and is a direct result of grain boundary instability manifested as grain boundary sliding coupled with rotation, grain coalescence and viscous flow. Further, such extreme behavior is only possible because the geometric softening that constitutes the formation of non-uniform deformation at elevated temperatures is suppressed by the high degree of strain-rate hardening allowing continuous deformation without fracturing. This universal phenomena has been well established since the early 1960's and though the underlying mechanism is still not fully understood, the general physical response has been described by the following constitutive equation [2].

$$\dot{\varepsilon} = A\frac{DGb}{KT}\left(\frac{b}{d}\right)^{p}\left(\frac{\sigma}{G}\right)^{n} \tag{2.1}$$

Here $\dot{\varepsilon}$ is the steady-state strain rate, D is the lattice or grain boundary diffusivity, G is the shear modulus, b is the Burgers vector, K is the Boltzmann constant, T is the test temperature, d is the average grain size, p is the grain size exponent, σ is the applied stress, n is the stress exponent and A is a material parameter [3,4,8]. This theory suggests that the higher temperatures required to initiate the superplasticity in conventional micron sized grains can be lowered several hundred degrees, if the grain size is reduced to the nanoscale, i.e., in metals having an average grain size below 100 nm. In support of the theory, McFadden et al. reported for nanocrystalline Ni and Ni-Al alloys, both with average grain sizes from 20-100 nm, the lowest normalized superplasticity temperature for any known crystalline material at that time [4]. More recently, room temperature superplasticity has been shown to occur in nanocrystalline Cu where extreme

extensibility (elongations exceeding 5000%) without strain hardening was reported by Lu et al. [3]. These finding are usually explained by postulating that superplasticity in NC materials is controlled by grain boundary mediated deformation mechanisms, such as grain boundary sliding and rotation [33].

Overall, the superplastic behavior is intensified in NC materials due to the increase in grain boundary volume fraction as compared to coarse grained materials [34]. As a result, NC materials exhibit superplastic behavior even at room temperature and/or high strain rates due to the very same grain boundary instabilities (i.e. grain boundary sliding, rotation and grain coalescence) arising in coarse grained superplastic materials at high temperatures [33]. However, contrary to conventional belief and hitherto, we present here extensive experimental and computational evidences that the low temperature superplastic flow, in truly stabilized NC (grain size 100nm or less) materials is inaccessible, i.e., NC materials that maintain an average grain size < 100nm at elevated temperatures will lack the necessary superplastic flow. We show that this unexpected trend is caused by stabilization of the grain boundary regions through interactions with nano-clusters, leading to elimination of grain boundary sliding and rotation (the predominant mechanisms governing superplasticity in NC metals) even near the melting point of the alloy. We further present that the NC material studied here exhibits a *limited* rate of strain hardening i.e. a mechanically elastic perfectly plastic response along with minimal texture changes (i.e., changes in the grain size, morphology and orientation). Finally, the deviation from the established superplastic behavior leads to a strong enhancement of high temperature mechanical properties. For example, a high temperature

strength is remarkably maintained up to temperatures as high as 80% of the melting point (~1356 K). Thus, our results demonstrate that selective grain boundary segregation of nano-clusters can be an effective design strategy for developing advanced materials for various applications.

2.2 Material Processing

The NC Cu-10 at.% Ta alloy (referred to herein as NC Cu-Ta) used in this study was produced through high energy ball milling followed by equal channel angular extrusion (ECAE) [35,36]. Elemental Cu and Ta powders (-325 mesh and 99.9% purity) were loaded into a hardened steel vial in the appropriate proportion along with the milling media (440C stainless steel balls) inside a glove box with an Ar atmosphere (oxygen and H_2O are < 1 ppm). The vials were loaded with 10 g of the Cu-Ta powder as well as the appropriate amount of media to ensure a ball-to-powder ratio of 5-to-1 by weight. A SPEX 8000 M shaker mill was utilized to perform the milling at cryogenic temperature (verified to be ~ -196 °C) for 4 hrs using liquid nitrogen. The NC-Cu-10at.%Ta powder was consolidated to bulk via equal channel angular extrusion (ECAE). Before starting the ECAE process, the die assembly used for processing the billets was preheated to 623 K (350 °C) to minimize thermal loss during the ECAE processing. The billets, heated and equilibrated to 973 K (700 °C) for 40 min, were dropped into the ECAE tooling as quickly as possible from the furnace and extruded at an extrusion rate of 25.5 mm/s. These steps were repeated 4 times following route Bc [37–39] to prevent imparting a texture to the consolidated powder. By extruding through an angle of 90°, a total strain of 460% was imparted onto the powder-containing billet as a result of processing.

Specimens for mechanical testing were then machined from these billets, within the region containing the consolidated powder, via wire electric discharge machining into 3 mm length by 3 mm diameter cylinders. Further details related to the processing and impurity levels can be found in [13,36,40,41].

2.3 Mechanical Testing

Conventional compression tests were performed over a wide range of applied deformation rates (10^{-4}- 1 s^{-1}) and temperature conditions (297 K - 1273 K). Quasi-static compression tests of specimens over a temperature range from ambient up to 1073 K (800 °C), were performed using an Instron load frame equipped with a 50kN load cell and an ATS clam-shell heating furnace capable of a maximum temperature of 1473 K (1200 °C). The specimens for compression were cylinders 3 mm in diameter and length (aspect ratio 1.0). Compression tests were conducted at 298, 473, 573, 873, and 1073 K, with strain rates ranging from 8×10^{-4} to 1 s^{-1}. The system was held at the testing temperature for 30 min prior to loading to provide uniform temperature within the specimen. The push rods of the load frame were constructed of Inconel 718. Polished WC-disks lubricated with graphite were used as platens for compression testing. A thermocouple embedded in the Inconel rod was used to measure the temperature of the specimen. The stress-strain responses are provided in Figure 1. The compressive curves display an elastic- nearly perfectly plastic behavior over the entire temperature with no significant strain hardening beyond 2.5% strain. Scanning electron images confirmed that a negligible oxide film (< 10 μm in thickness) was formed on the surface of the cylinders as a result of exposure to the elevated temperatures, as measured post testing.

2.4 Characterization

To obtain grain size distributions and microstructural characteristics, Transmission Electron Microscopy (TEM) was employed. TEM characterizations were carried out in the as-received and post-deformed conditions using an aberration corrected ARM-200F at 200 KeV. Multiple bright field and dark field images were captured in both the high resolution TEM and STEM modes to assess the microstructure and quantify statistics such as grain size distribution etc. For TEM characterizations, samples were prepared through conventional thinning procedures where a 3 mm disk from the bulk specimen was thinned to about 70 μm following which the specimens were dimpled to about a 5 μm thickness. Ion milling was performed using a Gatan Precision Ion Polishing System (PIPS) under liquid nitrogen temperatures to obtain electron-transparent regions in the specimens. The samples were also plasma cleaned in Ar prior to TEM observations to reduce contamination.

Primary microstructural characterization using TEM revealed the presence of nanocrystalline grain sizes for the copper and tantalum particle phases with an average grain size of 50 ±18 nm for Cu. Tantalum particles are shown to exhibit a range of sizes from atomic sized clusters ($d < 14$ nm) to larger particles ($d > 14$ nm). The larger particles and atomic sized clusters have an average diameter of 32 ± 8 nm and 3.18 ± 0.9 nm, respectively. The size distributions were obtained from areas similar to that seen in the Extended Data Figure 2 of [36], which was averaged over 300 grains. It is important to note that the microstructure has a few twins, but the formation of nano-twins during

processing for this composition is minimized due to the presence of fine nanoclusters[41].

2.5 Results

This alloy was studied previously in limited mechanical testing such as a high temperature creep study where the sample is tested within the elastic limit as compared to the superplastic behavior probed here tested in the inelastic regime [35,36]. Typical true stress-strain curves are shown in Figure 1A. Inspection of these curves reveals several significant findings. First, the absence of appreciable strain hardening (i.e., elastic-perfectly plastic behavior) at various deformation rates and temperatures suggests that no significant changes in grain size, morphology or texture occurred during the deformation. Secondly, the strain rate sensitivity (m) is negligible at the room temperature; however, as the applied temperature is increased, the rate effects become more apparent.

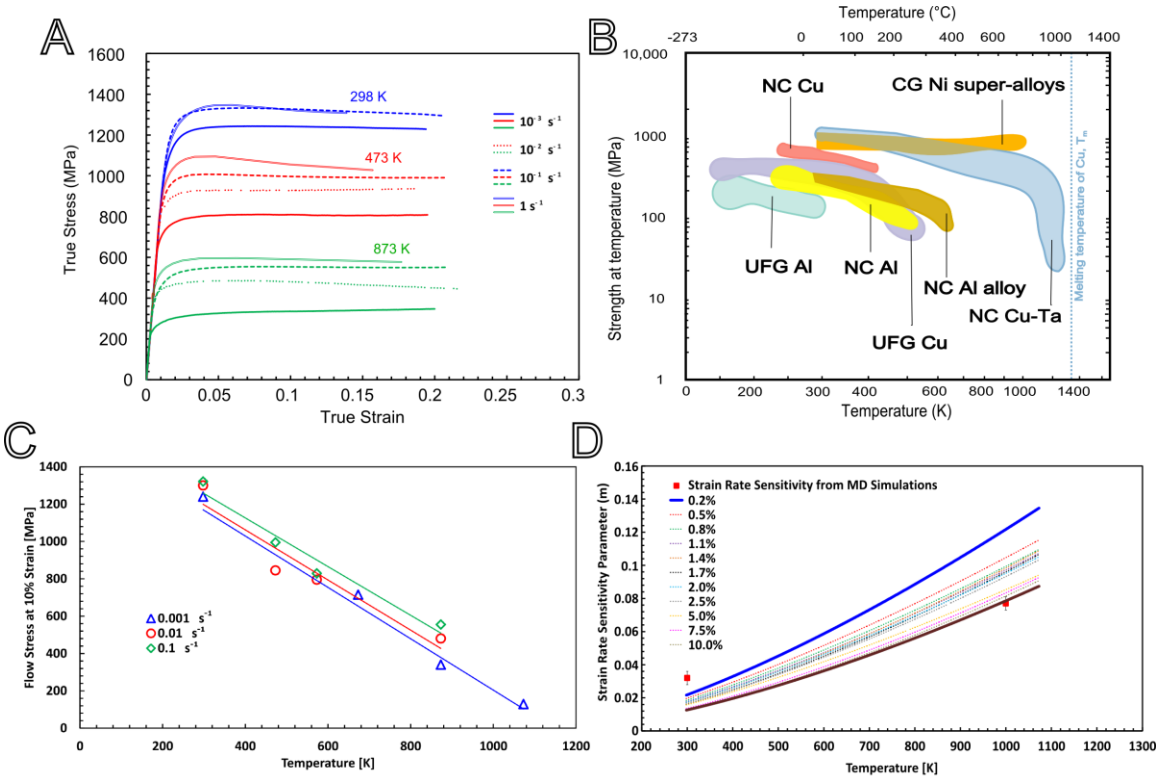

Figure 2.1 Thermal dependence of NC-Cu-10at.%Ta. a) The low strain rate stress-strain response of NC-Cu-Ta as functions of strain rate and temperature, b) strength (yield stress for NC-Cu-Ta from (a)) at temperature versus applied temperature for NC and UFG metals and alloys, c) linear behavior of flow stress as a function of temperature for NC-Cu-10at.%Ta, and d) influence of temperature on strain rate sensitivity at various strain levels in NC-Cu-Ta along with molecular dynamic simulation results.

Next, the 0.2% yield strength evolution of the NC Cu-Ta alloy in comparison to other NC, ultra-fine grained (UFG) and CG material systems are shown in Figure 1B as an Ashby plot of strength versus temperature. The upper and lower bounds of the individual contours correspond to the stress response within the strain rate limits (0.001- 1 s^{-1}) over the given temperature range (Figure 1A). For instance, the strength of the NC Cu-Ta alloy at 200 °C under compression was found to be 650 MPa and 925 MPa for the strain rates of 0.001 and 1 s^{-1}, respectively. Thus, a significant fraction of the room temperature strength (59 and 76%, respectively) was retained. Even under more intense conditions,

this alloy demonstrates a remarkable thermal-mechanical stability wherein the yield and flow stresses follow a linear decrease with temperature (Figure 1C). This is in stark contrast to the expected sigmoidal temperature dependence demonstrated by CG Cu and Cu-based alloys. Further, as shown in Figure 1, the rate of stress decreases with the rise in temperature which occurs much earlier for conventional NC and UFG materials. In fact, in comparison, the temperatures at which the current generation NC and UFG materials are tested can be deemed low as the service temperatures for the operation of structural components are significantly higher. However, NC Cu-10at.%Ta exhibits a higher resistance to the influence of temperature which is contrary to the reported literature.

The observed retention of strength at elevated temperature raises a critical question: is there a strain hardening and/or superplastic behavior at such temperatures? To address this, the strain rate sensitivity parameters m obtained from the slopes of several plots of $\log \sigma$ vs $\log \dot{\varepsilon}$ are shown in Figure 1D as a function of strain and temperature. The strain rate sensitivity is an indicator of changes in deformation behavior and is inversely proportional to the activation volume. The latter is a critical parameter for determining the rate-controlling step of the plastic deformation mechanism in the material, since it has a different value and stress dependence for each atomic process. Figure 1D can then be used to observe the evolution of the rate-controlling mechanisms with strain and temperature in the NC Cu-Ta alloys. The yield stress of a material is known to be more dependent on strain rate at lower strain values [2] and this is consistent with the data presented in Figure 1D, where the m values calculated at lower strains are higher than m

values calculated further along the stress strain curves. At elevated temperatures, this rate dependence at lower strains is more prominent as indicated by the 5 fold increase in the spread of the m values over the given strain range (i.e., 0.2 – 12.5 %). This indicates the more pronounced role played by the thermally activated strain hardening processes in dictating the strain rate sensitivity at early stages of deformation. Further, as expected, the strain rate sensitivity increases for all strains with temperature by almost a factor of 10. However, despite the significant increase, the magnitude of the strain rate sensitivity parameter m does not break the threshold expected for superplasticity (above 0.3).

The average value of m for the NC-Cu-Ta alloy taken at 1073K is 0.087, which corresponds to an apparent activation volume of $v^* \sim 60b^3$. v^* is a direct measure of the average volume involved with the specific deformation process. When deformation is controlled by processes such as grain boundary sliding, rotation and diffusional creep, the v^* is relatively small, generally in the range of 1-10 b^3. This is consistent with literature values for superplastic materials where v^* is typically ~ $2b^3$ [42]. For comparison, conventional FCC metals generally have very large v^* values (100's-1000's of b^3), wherein the deformation is associated with dislocation cutting through forest dislocations. The small v^* values close to $1b^3$ are associated with atomic displacements/jumps i.e. viscous flow indicative of the process required for sustained deformation. An extensive survey of over 184 alloys based on Zn, Sn, Mg, Al, Cu, Fe, Ni and Ti has shown that the alloy with the stable grain sizes ~ 10 to 400 times larger than in the NC-Cu-Ta alloy (i.e. grain sizes of 1 to 20 □m), all are superplastic (m values between 0.3-0.8) at homologous temperatures between 50 and 80% T_M [42]. The observations made here on NC-Cu-

10at.%Ta go against the general constitutive relationship of reduced grain size, elevated temperatures and strain rate. It would be expected that such a small grain size at such a high temperature (50 - 85 nm and 873 - 1073K or 64 - 80% T_M) would give rise to ultra-high strain rate superplasticity. Instead, the behavior found here is the direct opposite to this expectation.

The plastic deformation in NC-Cu-10at.%Ta tested here was determined to occur either through deformation twinning or dislocation slip. Studies have indicated that GBs serve as the origin for nucleation and provide a point for storing and annihilating/absorbing dislocations after they transverse the grain under an applied stress. These GBs are also responsible for pinning the dislocations ultimately obstructing their motion by strongly influencing when and where cross-slip can occur and by increasing the energy to unpin and move across to the neighboring grains [43–46].

To investigate the active deformation mechanisms and the reasoning behind the high temperature and strain rate response in these alloys, ex-situ microstructural characterization was employed using the same techniques employed to investigate the as received microstructure. In general, the emissions of partial and full dislocations are competing mechanisms and their activation depends on the stress level and testing temperature. From the TEM observations presented here (Figures 2 and 3) on NC-Cu-10at.%Ta, an appreciable dislocation density can be identified for quasi-static testing conditions implying an absence of dislocation absorption. In the case of conventional nanocrystalline materials, grain boundaries act as a source for dislocation generation. The dislocations are then free to traverse the grain and be absorbed at the opposite grain

boundary which acts as a sink. In the NC-Cu-10at.%Ta alloy, the dislocations are emitted, interact with the high density nanoclusters, and become pinned at various sites, thereby, reducing the mean free path for the propagation of the dislocations.

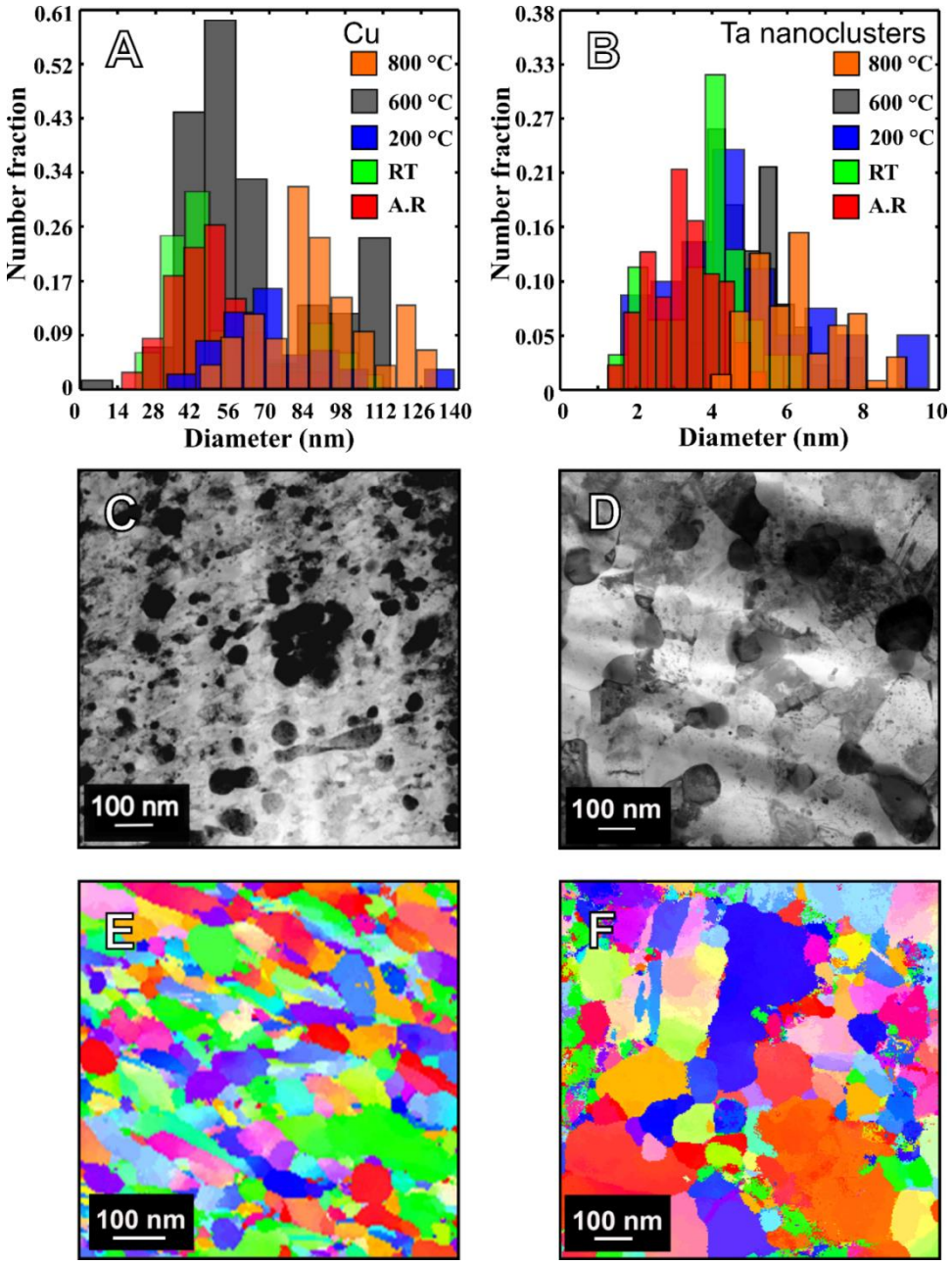

Figure 2.2 Grain size distribution of Cu and Ta nanoclusters obtained from as-received and quasi-static tested samples (at 0.01 s^{-1}). a) The distributions indicate nominal increase in grain size for Cu with majority of the grains in the nanocrystalline regime. b) Ta nanoclusters also exhibit stability with temperature. c) BF image of as-received sample. d) BF image of quasi static (0.01 s^{-1}) tested sample at 1073 K. e) precesion diffraction image of as-received sample. f) precesion diffraction image of quasi-static (0.01 s^{-1}) tested sample at 1073 K.

The observed unique hardening behavior of the NC Cu-Ta alloy raises the question: are there any microstructural changes in this material at elevated temperatures? To address this question, we performed a high resolution TEM characterization of grain size and crystallographic orientations as a function of temperature. Figure 2A-B shows grain and Ta cluster size distribution plots, which indicate very little change in either, despite being exposed to temperatures above the consolidation temperature of 973 K. The distributions reveal an increase in the grain size from 48.5±16.1 nm in the as-received condition to 89.7±12.8 nm after the 0.01 s^{-1} tested at 1073 K (0.8 T_m). In general, the matrix grains were found to be equiaxed in shape and coexist with larger residual Ta particles, spheroidal in morphology, having an average diameter of 32 nm for both samples (Figure 2C). Such small changes in the microstructure are very surprising given that the average grain size is less than 100 nm at the deformation temperature of 1073 K. To evaluate the influence of the deformation rate and temperature on the textural changes, we further performed precession diffraction which are shown in Figures 2D-E. The as received orientation imaging map (OIM) illustrates a high degree of randomness in the orientation relationship between the grains of the NC Cu matrix (see the inverse pole figure). It also indicates the density of specific orientations or multiples of the uniform distribution (MUD) to be 1, which is consistent with being random in nature. The same is true for the 1073 K post-tested sample (Figure 2E).

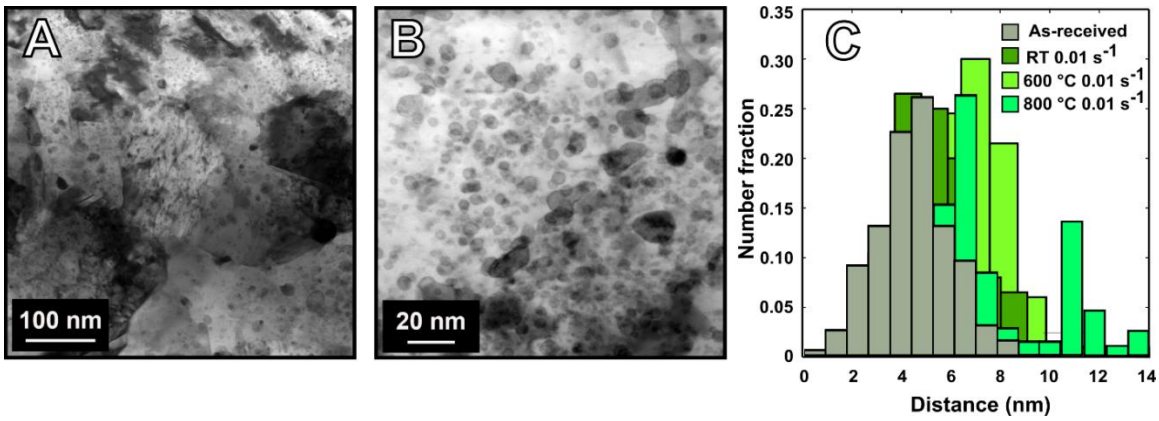

Figure 2.3 BF images of quasi-static (0.01 s^{-1}) tested sample at 1073 K showing nanoclusters along with the average inter cluster spacing distribution. a) BF image of quasi-static (0.01 s^{-1}) tested sample at 1073K b) Higher magnification BF image showing distribution of Ta nanoclusters. c) Inter cluster spacing distribution for as-received sample along with quasi-static (0.01 s^{-1}) tested samples at RT, 873K and 1073K.

Following the divergence in the observed behavior, we turn to further microstructural characterizations illustrating the role of nano-clustering on the mechanical behavior. As illustrated in Figure 1, this unusual thermo-mechanical response stems from the retention of the NC grain structure. To better understand the origin of this behavior, higher magnification aberration corrected STEM was used to resolve, in more detail, the underlying microstructural features. Figures 2C-D and 3A-B illustrate the archetype microstructure of the present material, where the Ta nano-clusters are distributed homogeneously along the grain interiors and at grain boundaries and interact with dislocations. The average size of the nanoclusters was found to be ~2-4 nm in diameter with an average inter-cluster spacing of 5.23 ± 1.74 nm. These numbers remain nearly constant with the application of stress and temperature, highlighting the stability and resistance to coarsening (see Figures 2B, and 3C). Thus, the stability of the Cu grains (Figure 2A) remains intact owing to the stability of the high density of coherent

nanoclusters present in the microstructure (Figures 3A-3B). These nanoclusters pin the grain boundaries and block the grain boundary sliding and grain rotation processes required for superplastic deformation. It is this pinning of the grain boundaries that is responsible for imparting the extraordinary strength and structural stability in these alloys, resulting in the anomalous mechanical response, namely, the breakdown of the universally expected superplastic behavior in NC materials.

As seen in Figure 1C, the flow stress results for both low and high strain rates reveal an apparent linear temperature dependence [1,12] as compared to the sigmoidal manifestation expected for pure, coarse grained Cu. In pure, coarse-grained Cu, the values of the flow stress are a result of thermally activated dislocation motion, where an increase in temperature increases the energy of the dislocation and lowers the activation energy that the dislocation must overcome to propagate. Thus, the flow stress (σ_f) decreases with temperature following an Arrhenius relationship as seen below (also refer to [47]).

$$\sigma_f = Ce^{\frac{-Q}{RT}} \tag{2.2}$$

where C is a constant, Q is the activation energy, R is the ideal gas constant, and T is the temperature. However, for NC-Cu-10at.%Ta, the flow stress is seen to decay near linearly as temperature increases. Moreover, the Cu grain size in NC-Cu-10at.%Ta after testing at 1073 K (800 °C) was estimated to be about 90 nm [13], indicating that grain coarsening is very limited and the reduction in observed yield and flow stress is solely dependent on increased thermal softening. In other words, the stable microstructure of the

NC-Cu-10at.%Ta alloy retains close proximity of dislocation barriers such as grain boundaries and nanoclusters such that these act as short range barriers to dislocation motion [2]. As increased temperature aids in overcoming short range barriers through increasing the vibration of dislocated atoms while long range barriers (e.g., grain boundaries) remain stable, the stress required to further deform the specimen (i.e., flow stress) decreases linearly. Thus, NC-Cu-10at.%Ta exhibits an extremely stable microstructure and unusual mechanical properties.

2.6 Conclusion

In an effort to retain a nanocrystalline grain size (i.e. < 100 nm), intense research efforts have focused on stabilizing grain boundaries through the kinetic and thermodynamic factors [9,48]. In particular, the interactions of solutes and secondary phases with grain boundaries can have a profound effect on the inherent mechanical properties and can challenge the long established theoretical frameworks related to mechanical behavior of materials, including the extreme creep resistance and increased plasticity [49]. In the light of these recent findings, we examine the question of whether stabilized NC materials will still manifest lower temperature superplasticity. The general view, until this point, has been to expect that such materials would be superplastic starting with lower homologous temperatures in comparison with coarse grained materials. However, experimental evidence reported here reveals that NC Cu-Ta (grain size < 100 nm) at high homologous temperatures and despite the absence of strain hardening, grain growth or texture formation, cannot achieve the necessary strain sensitivity m > 0.3 to be considered superplastic. These observations imply that, to the

contrary of conventional belief, a truly stabilized NC material will not exhibit superplastic behavior even when subjected to temperatures as high as 80% of the melting point. Thus, by suppressing the grain boundary processes through complex grain boundary nanocluster interactions, the paper highlights a unique materials design aspect through which materials with extraordinary strength (approximately one half the theoretical limit) and high temperature stability can be developed for advanced technological applications. In summary, this works opens a new frontier towards developing structural and functional materials that have been difficult to achieve via conventional techniques.

3 ANOMALOUS MECHANICAL BEHAVIOR OF NANOCRYSTALLINE BINARY ALLOYS UNDER EXTREME CONDITIONS

Fundamentally, material flow-stress increases exponentially when the deformation rate reaches ~10^3 s^{-1}, resulting in brittle failure for most metals. The origin of such behavior derives from a classical abstraction that dislocation-motion causes non-Arrhenius deformation at higher-strain-rates due to internal-drag-forces from phonon interactions. In this study, we discovered that this simple assumption, established 50-years ago, does not apply when the average grain size and microstructural length-scale is decreased below 100 nm. This divergent strain-rate behavior is attributed to a unique microstructure that limits the mobility of dislocations such that dislocation velocity cannot exceed the velocity required for phonon interaction to play a significant role on the flow stress. Hence, the present study provides a pathway for designing and synthesizing a new-level of tough and high-energy absorbing materials.

3.1 Introduction

A material's ability to withstand high deformation rates without failure has a profound effect on everyday applications, indeed, in modern industrial society, e.g., in the case of, alternating energy supply (fusion reactors), and during automobile crashes, projectile impact, shock loading, and deep-space exploration (space debris and meteorite impact) structural metals often experience sudden deformation rates of 10^3-10^8 strain-per-second or higher. Generally, almost all metals, structural and functional, show a dramatic upturn in flow stress when the strain rate reaches ~10^3 s^{-1} [50–54]. This distinctly

different non-Arrhenius dependent regime is in part due to dislocation interactions with thermal fluctuations, commonly known as phonon-drag, which limits the materials' ability to plastically deform prior to failure. Thus, engineers have been in a quest to improve the fracture toughness of conventional (coarse) grained metals and alloys, i.e., whether a material can be designed that will deform with a constant flow stress even when subjected to extreme conditions of pressure, and high rates of loading [55]. In other words, does the material plastic response remain the same under various loading rates? For such behavior to manifest, the long-established mechanism of phonon-drag leading to flow stress increase must break down. However, the intensity of the deformation rate, which can vary by 8 orders of magnitude depending on how the load is applied, complicates the design and processing of coarse grained metals.

On the other hand, where the development of conventional grained metals has fallen short in engineering enhanced properties, nanocrystalline (NC) metals, i.e., metals having an average grain size < 100 nm, hold new promise. In other words, in regimes where thermally activated processes strongly control the deformation behavior (below 10^0 s^{-1}), NC materials [36,56,57] have emerged to display enhanced/unusual grain size dependent behavior such as high room temperature strength [34]. However, until now, the same type of deviating mechanical responses that have been found to exist in the thermal activation regime have not been shown to manifest under conditions where the applied stresses are high enough to overcome the usual dislocation barriers without aid from thermal fluctuations. In other words, the limited room temperature high strain rate studies in NC materials have observed similar increased flow stress above 10^2-10^3 strain-per-second as

in coarse grained materials [18,58,59] due to microstructural instability. In the following, we present evidence that the long-established mechanism of phonon-drag leading to flow stress increase does not apply to stable NC materials, even up to temperatures as high as 473 K (or $0.35T_m$ for Cu where T_m (1,356 Kelvin) is the melting temperature of the matrix) where the drag coefficient should be much higher based on Bose-Einstein statistics of phonon frequency [21]. Previously, these extreme regimes of loading conditions were unattainable in NC materials without a loss of the NC structure due to thermal and mechanical instability; thus, the delayed flow stress increase has never before been observed even at room temperature.

3.2 Materials and Methods

Nanocrystalline (NC) Cu-10at.%Ta powders were processed following the procedure outlined in Chapter 2. Specimens for mechanical testing were machined from the NC-Cu-10at.%Ta billets, within the region containing the consolidated powder, via wire electric discharge machining into 3 mm length by 3 mm diameter cylinders. Details related to the processing and impurity levels can be found in [13,36,40,41]. This alloy was studied previously using limited mechanical testing methods, such as high temperature creep [36] where we used this NC alloy to assess the response of a material under high temperatures.

To obtain grain size distributions and microstructural characteristics, Transmission Electron Microscopy (TEM) was employed. Details regarding specimen preparation and imaging are listed in Chapter 2.

Atom probe tomography (APT) was performed using a Cameca Local Electrode Atom Probe (LEAP) 5000 XS instrument. The specimens were lifted-out from the sample ECAE processed at 700 °C and placed on a pre-fabricated Si post using an FEI Nova 600 NanoLab dual-beam scanning electron microscope and focused ion beam (SEM/FIB) equipped with an Omniprobe micromanipulation system. Once welded to the Si post, each specimen was annular milled to a final tip diameter of 60-100 nm. During the APT experiments, the specimens were maintained at a base temperature of 45 K (-228°C) and run in the pulsed laser mode with a pulse rate of 333 kHz, pulse energy of 50 pJ, and a target evaporation rate of 0.5%. The APT data was reconstructed using Cameca's Integrated Visualization and Analysis Software (IVAS) 3.6.12. The mechanical alloying followed by ECAE processes resulted in a microstructure consisting of an average grain size of 50±18 nm and an average twin width of ~10.38 nm for Cu along with Ta based nanoclusters having an average diameter of 3.2±0.9 nm and an inter-cluster spacing of 4-to-7 nm.

Procedures for quasi-static compression tests of specimens over a temperature range from ambient up to 1073 K (800 °C) are detailed in Chapter 2. High strain rate compression tests of specimens over a temperature range from ambient up to 1073 K (800 °C) were performed using an Inconel 718 Kolsky bar with 12.7 mm diameter and a tube furnace capable of reaching a maximum temperature of 1173 K (900 ˚C). The specimens for compression high-strain rate testing were also cylinders 3 mm in diameter and length (aspect ratio 1.0). Tests were conducted at various temperatures ranging from 298 to 1073 K (25 to 800 °C) with strain rates ranging from 1×10^3 to 2×10^4 s^{-1}.

Details about the Kolsky bar test were previously discussed in chapter 1, so they will not be further discussed here.

As a result of the short deformation time during Kolsky bar testing, force equilibrium on each side of the specimen is not attained until plastic deformation has already begun. Further, at high strain rates and high strain levels, adiabatic heating causes softening in samples, so flow stress should be determined at low levels of strain. Since the samples consistently reach equilibrium by 10% strain, flow stress is taken at a 10% strain level and the rise in temperature resulting from adiabatic heating as determined by the method of Kapoor and Nemat-Nasser [28] was calculated. Assuming 100% of the work in the sample is converted to heat at the 10% strain level, adiabatic heating causes less than an approximately 40 °C rise in temperature at testing temperatures below 473 K (200 °C) and less than approximately 20 °C for testing temperatures above 473 K (200 °C).

The yield stress determined from Taylor anvil experimenting is merely an estimate and finite element simulations are needed to determine more accurate values of the flow stress at strain rates above 10^4 s^{-1} [60]. To this end, finite element simulations based on a Johnson-Cook model [61] with parameters listed in Table 3.1 are shown to result in a reasonable fit to the lower strain rate data for NC-Cu-10at.%Ta.

Table 3.1 Johnson-Cook Parameters for NC-Cu-10at.%Ta

A	1,229 MPa
B	303 MPa
n	0.264
C	0.01
$\dot{\varepsilon}_0$	1 s^{-1}

3.3 Results

Primary microstructural characterization using TEM (Figure 3.2) revealed the presence of nanocrystalline grain sizes for the copper and tantalum particle phases with an average grain size of 50 ±18 nm for Cu. Tantalum particles are shown to exhibit a range of sizes from atomic sized clusters (d < 14 nm) to larger particles (d > 14 nm). The larger particles and atomic sized clusters have an average diameter of 32 ± 8 nm and 3.2 ± 0.9 nm, respectively. The size distributions were obtained from areas similar to that seen in the Extended Data Figure 2 of [36] and were averaged over 300 grains. It is important to note that the microstructure has a few twins, but the formation of nano-twins during processing for this composition is minimized due to the presence of fine nanoclusters [41].

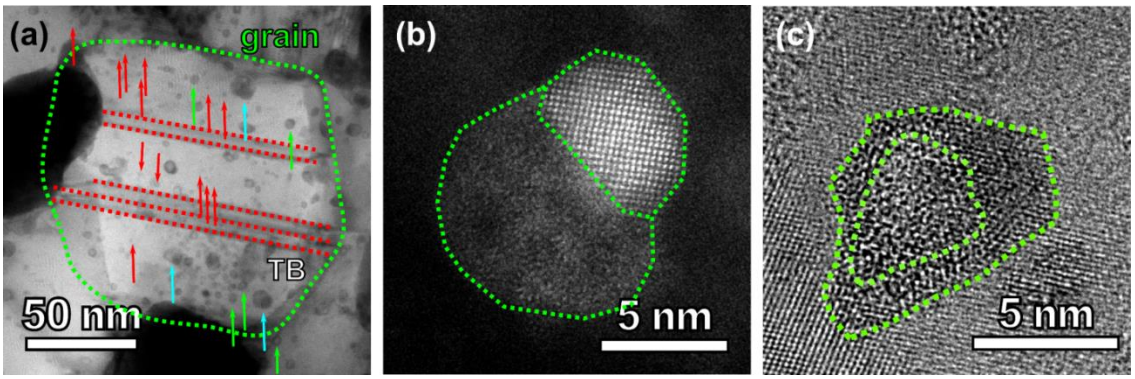

Figure 3.1 As-received microstructural characterization. a) Bright field STEM image indicating the features of as-received NC-Cu-10at.%Ta such as twins, and the structure and distribution of nanoclusters. The red arrows are for smaller nanocluster sizes followed by green and blue for larger sized ones. b) HR-STEM HAADF image of a co-joined nanocluster with crystalline and distorted components of the nanocluster. The interface between the components and matrix is highlighted in green dashed lines. c) HR-TEM image of another type of nanocluster with a core-shell morphology where the shell is crystalline and the core consists of defects such as vacancies.

Figure 3.3 shows the 3-dimensional reconstructed tip of NC-Cu-10 at% Ta from APT measurements. The orange spheres are the Cu ions of the matrix material, while the green surfaces identify and mark the large particles of Ta present within the alloy system. (These regions are delineated from the matrix of the alloy using a TaO isoconcentration surface set to 7.28 at% TaO, where the interior of the surface has a higher concentration of Ta and O compared to the lower content outside the surface in the Cu matrix). Two of these smaller isoconcentration surfaces had 1-dimensional concentration profiles run through them to measure the partitioning behavior of Cu, Ta, and O within them. This yielded some interesting results that correlate nicely with the variety of Ta particles present in the TEM micrographs shown in Figure 3.2. One of the 1D profiles indicates the particle has a core-shell structure. This is seen by the O composition reaching a maximum where the Ta composition decreases and the Ta composition reaching its maximum on both sides of this O peak. This signifies an outer shell that is enriched in Ta, and as the core is reached, the Ta content decreases as an increase in O occurs. This particle is ~ 5 nm in diameter. When performing the same analysis on a slightly smaller (~2-4 nm) surface, the O and Ta composition reach their maximum compositions at the same point. This indicates the core-shell structure is not present in this particle, which corresponds to the variety of particle structures seen in the TEM micrographs with smaller particles displaying a more constant contrast across themselves indicative of a uniform composition and large particles having a changing contrast due to a chemical compositional change. Figure 3.3c-d reveals an image taken from the interior of a smaller

particle showing the clustering of Ta and TaO particles within the interior of the isoconcentration surface compared to the surrounding matrix of Cu ions.

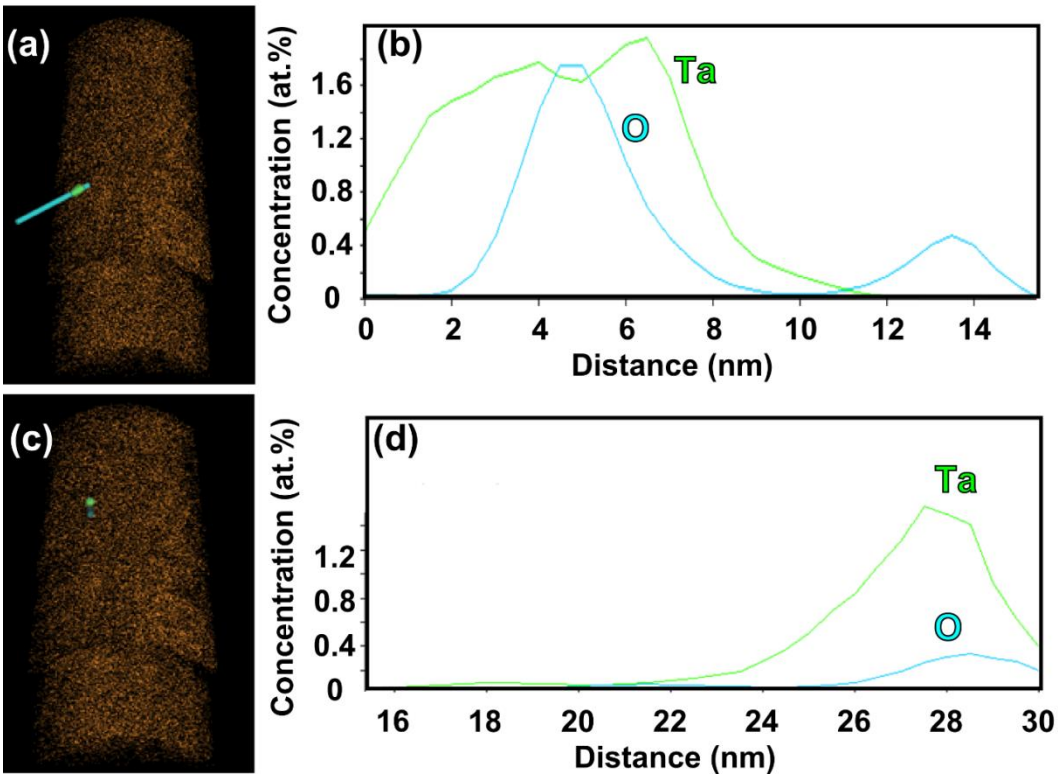

Figure 3.2 As-received microstructural characterization. a) and c) Atom probe reconstruction showing Cu ions, a Ta particle (delineated with a 7.28 at.% TaO isoconcentration surface), and an analysis cylinder placed within two different Ta particles b) and d) 1-dimensional concentration profile generated from the analysis cylinder showing the O and Ta concentration within the particle of a) and c).

The stress-strain responses are provided in Figure 3.4. The compressive curves display an elastic- nearly perfectly plastic behavior over the entire temperature range with no significant strain hardening beyond 2.5% strain. Very little strain rate sensitivity is apparent at 273 K, and even with a testing temperature of 473 K, the flow stress of the nanocrystalline material is around 1 GPa. Interestingly, despite the thermal dependence at

temperatures greater than 273 K, little rise in flow stress is observed as a result of decreasing the temperature to 223 K.

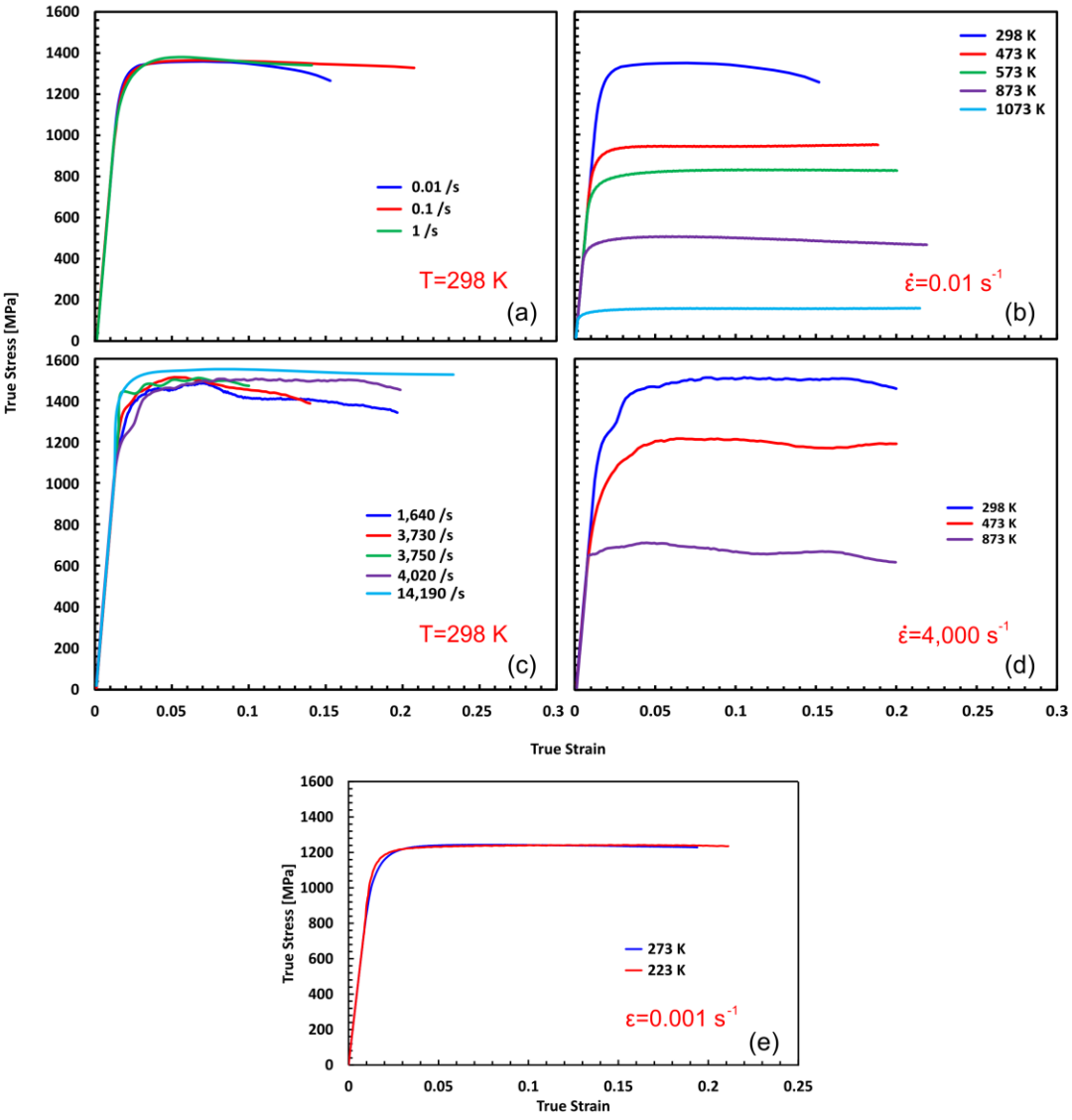

Figure 3.3 Stress-strain results at multiple strain rates and temperatures. a) Quasi-static compression at room temperature, b) 10^{-2} s^{-1} compression for temperatures ranging from room temperature to 1073 K (800 ˚C), c) high strain rate compression at room temperature, d) 4×10^{3} s^{-1} compression for temperatures ranging from room temperature (298 K) to 873 K (600 ˚C), and e) comparison of 10^{-3} s^{-1} compression at 273 K and 223 K for NC-Cu-10at.%Ta.

Taylor anvil results are shown in Figure 3.5. The finite element analysis (FEA), performed using a Johnson-Cook analysis with good fit to lower strain rate experimental data as seen in Figure 3.5a, accurately predicts the overall geometry of the post deformed experimental profile as shown in Figure 3.5b. The result revealed a flow stress of 1,500 MPa where the maximum strain rate measured one element from the impact surface is approximately 2×10^5 s^{-1}. This confirms the Taylor anvil experiment results (flow stress of 1,480 MPa at 10^5 s^{-1}) showing that no significant upturn in flow stress occurs at strain rates up to 10^5 s^{-1}.

A comparison of pure Cu and NC-Cu-10at.%Ta samples in Figure 3.5c reveals that the pure Cu experiences a higher degree of deformation than the NC-Cu-10at.%Ta indicating that the strength of the NC-Cu-10at.%Ta is much higher than that of the pure Cu despite the dramatic rise in flow stress observed in the pure Cu. This is a result of the inherent strength of the NC material, which is higher even than the pure Cu tested at 10^5 s^{-1}. However, when the estimated yield stress from the Taylor anvil experiment is normalized by the appropriate quasi-static 10% flow stress behavior, the increase in flow stress observed by the pure Cu sample is significantly higher than the flow stress increase observed by the NC-Cu-10at.%Ta sample which implies that the change in deformation mechanism which causes the upturn in pure Cu is not present in the NC-Cu-10at.%Ta up to a strain rate of 10^5 s^{-1}.

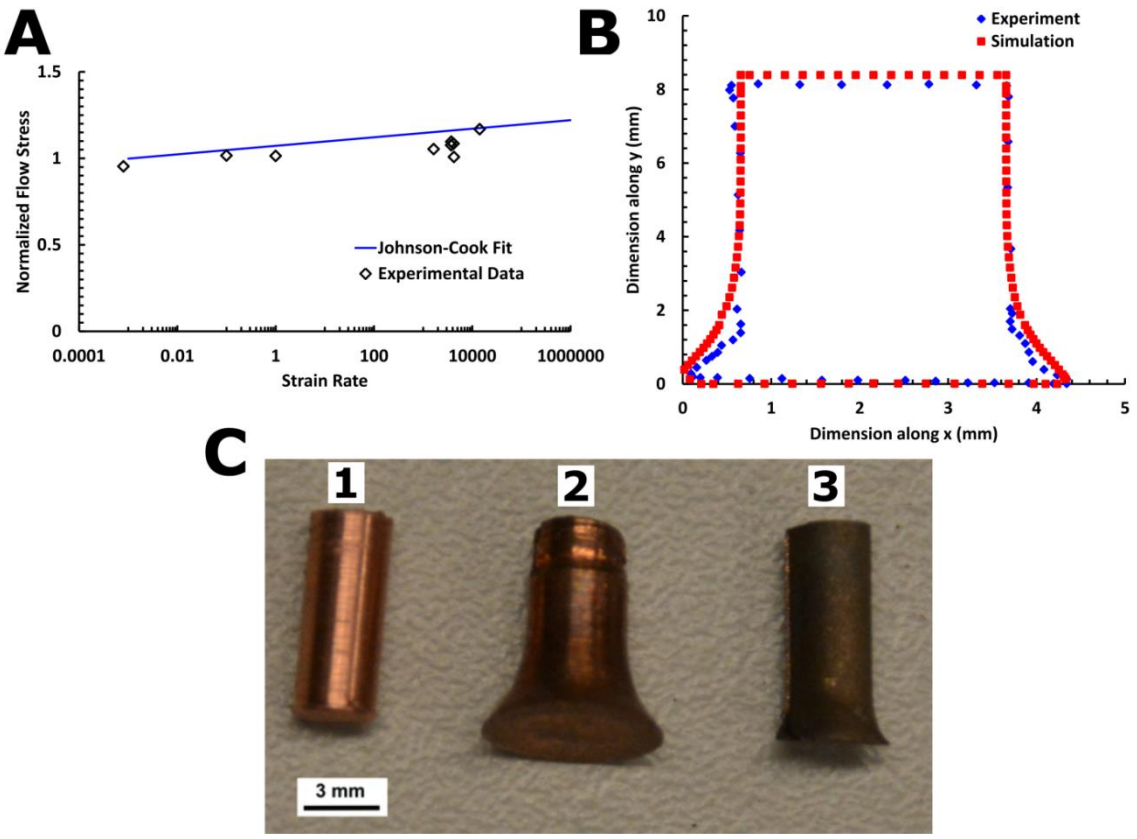

Figure 3.4 Fits of model to Taylor anvil experiment data. a) The flow stress as a function of strain rate for the experimental data obtained from quasi-static and Kolsky bar testing compared to the Johnson-Cook model fit with parameters from Table 3.1. b) Deformed geometry from the simulation is shown to match reasonably well with experimental results. The maximum strain rate obtained from simulations one element away from the impact surface measured approximately 2×10^5 s^{-1}. c) Samples from Taylor anvil experiments, which show representative specimens of: 1) an undeformed, pure Cu specimen, 2) the large deformation of a pure Cu specimen and 3) the relatively minimal deformation of a Cu-Ta sample.

To analyze the effects of temperature and stress on the macroscopic manifestation of phonon drag, conventional uniaxial compression tests were performed over a wide range of applied deformation rates (10^{-4} - 10^5 s^{-1}) and temperatures (223 – 1273 K) as discussed above. The NC-Cu-10at.%Ta alloy exhibits an especially high flow stress. Figure 3.6a represents a comparison of the flow stresses of various high purity Cu and Ta materials

representing differing grain sizes, and it can be clearly seen that the flow stress of the NC-Cu-10at.%Ta is higher than all other materials shown. Similarly, Figure 3.6b shows the flow stress results at a constant plastic strain of 10%, which are normalized with the flow stress obtained at a quasi-static strain rate of 10^{-2} s^{-1}, then plotted as a function of strain rate. A comparison of flow stress values taken from different strain levels can be seen in Figure 3.7 where little difference in normalized flow stress can be seen as a result of strain level for NC-Cu-10at.%Ta. The differences in flow stress as a function of strain level are also compared to polycrystalline Cu and Ta in Figure 3.7. Similarly, the normalized flow stress data for polycrystalline Cu [14], polycrystalline Ta [24], and coarse grained OFHC Cu obtained by Taylor impact [15] are also presented in Figure 3.6. A clear upturn in the flow stress, albeit initiating at differing strain rates, can be noted for polycrystalline Cu, NC-Cu, and polycrystalline Ta. The observed dramatic rise in flow stress is fundamental in origin and therefore common to all known structural metals with plasticity such as Cu, Fe, and Ta and believed to be the direct result of either the rise in the mobile dislocation drag force brought about by interactions with phonons in the crystal lattice or a sudden increase in the nucleation of dislocations. The fundamental theory of phonon-drag on mobile dislocation motion has been a seminal contribution in describing the mechanical behavior as a function of deformation rates despite microstructural differences for the past 50 years [62]. However, this prevailing theory does not apply to the NC material reported here, i.e., the general behavior of flow stress increase is absent even up to rates as high as 10^{5} s^{-1} where the flow stress upturn can be seen to play a more dominant role in the other material systems reported. For instance,

we find the room temperature flow stress at ~4.0×10^3 s^{-1} for pure Cu [14] and polycrystalline Ta [24] is increased by factors of 6 and 10, respectively, as compared to NC-Cu-10at.%Ta which indicates that the NC alloy is minimally influenced by either phonon-drag forces or increased dislocation nucleation. To further support observations of this behavior, we use the direct Taylor anvil experiment to extract approximate material behavior at strain rates closer to 10^5 s^{-1}, see the solid markers of Figure 3.6. The Taylor anvil experiment coupled with finite element analyses have been employed to qualitatively infer the strength of the material reported here for coarse grained pure Cu and NC-Cu-10at.%Ta. In this work, the room temperature dynamic behavior measured using the Taylor anvil experiment at 10^5 s^{-1} shows a negligible variation in the stress as compared to coarse grained pure Cu, asserting the observation of a flow stress behavior with, at the very least, a delayed onset of the flow stress upturn.

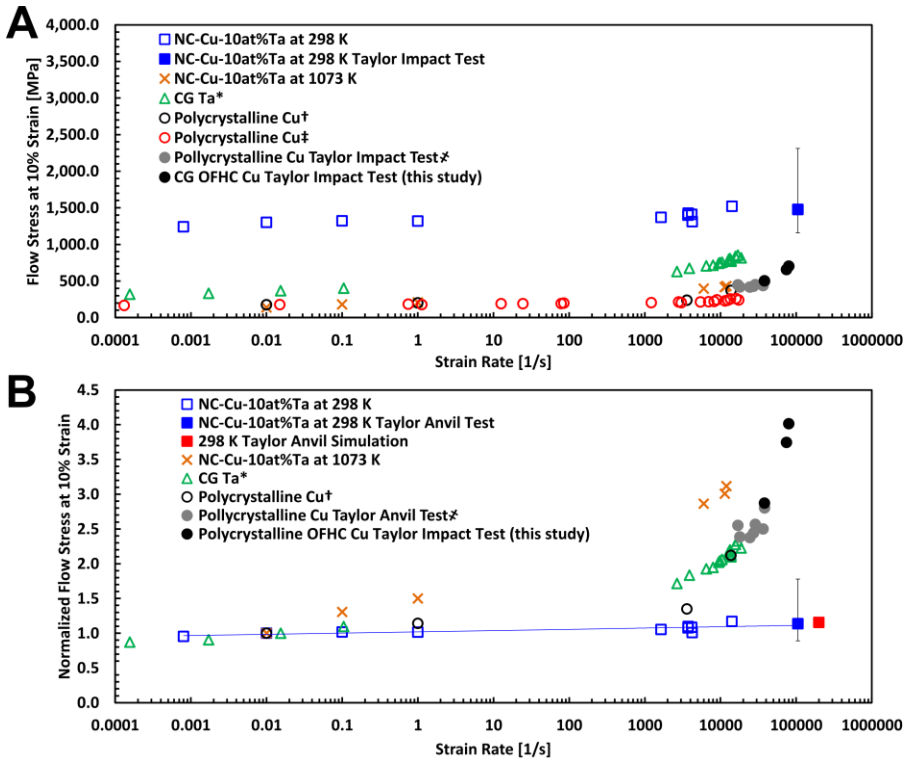

Figure 3.5 Flow stress-strain rate response of NC-Cu-10at.%Ta compared to polycrystalline Cu and Ta from literature. a) The high flow stress of NC-Cu-10at.%Ta compared to that of various pure Cu and Ta materials. The plots of non-normalized flow stress indicate the immense increase in strength resulting from alloying and grain reduction even up to strain rates on the order of 10^5 s^{-1} while the b) flow stress at 10% plastic strain normalized by the flow stress at 10^{-2} s^{-1} reveals the difference in flow stress upturn observed in the various samples. Data above 10^4 s^{-1} (solid symbols) was approximated using Taylor tests. Error bars in the Taylor anvil tested data represent analysis with $0.5 < f < 1$. Data on other materials are taken from Rittel et al. [24] (*), Jordan et al. [14] (†), Follansbee and Kocks [63](‡), and House et al. [15] (⊀). The power law fit for the Cu-10at.%Ta data reveals that the material is subject primarily to thermal activation processes up to a strain rate of 10^4 s^{-1}.

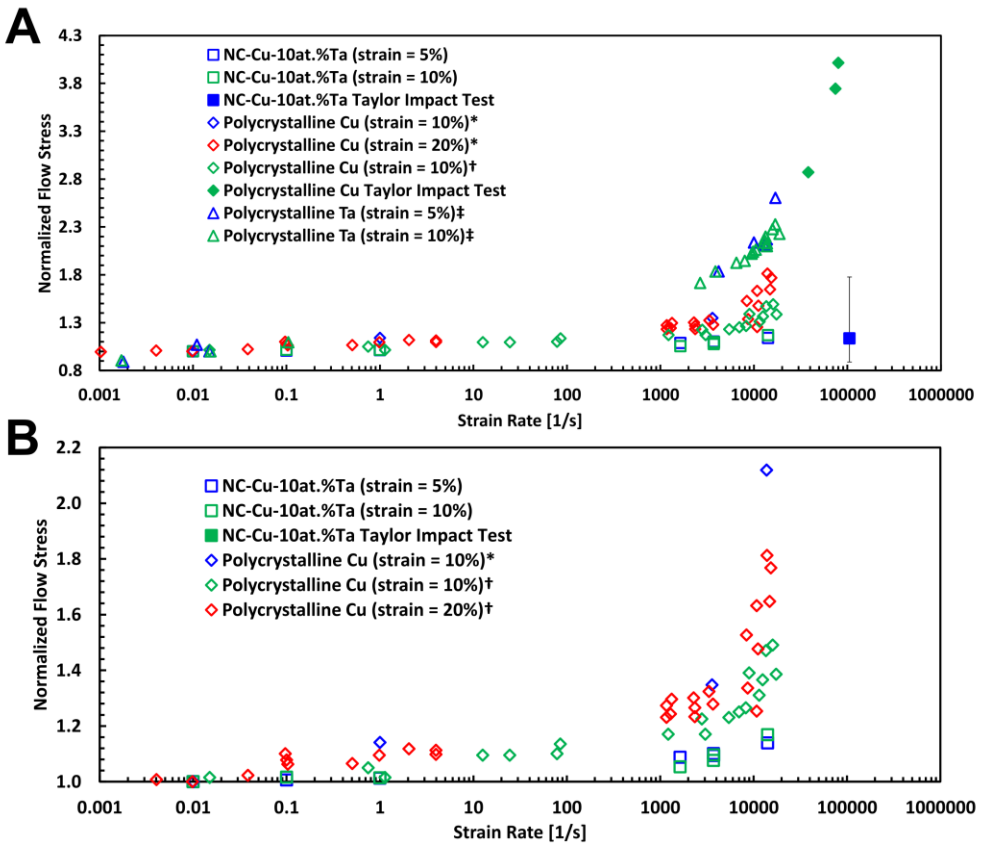

Figure 3.6 Flow stress-strain rate variation as a function of strain level. a) NC-Cu-10at.%Ta data taken at strains of 5 and 10% are compared with polycrystalline Cu from Jordan et al. [14] (*) at 10 and 20% strain as well as from Follansbee and Kocks [63] (†) at 10% strain. Also, polycrystalline Ta from Rittel et al. [24] (‡) at 5 and 10% strain. Limited variation is observed in normalized flow stress at each of the aforementioned strain levels. The NC-Cu-10at.%Ta data remains lower than the polycrystalline data and no upturn is observed in the data presented here. Error bars in the Taylor anvil tested data represent analysis with $0.5 < f < 1$. b) By removing the Ta and all Taylor anvil experiment data, the flow stress upturn in polycrystalline Cu is more clearly seen to occur at a lower strain rate than that of the stabilized NC-Cu-10at.%Ta.

Investigating the temperature dependence of flow stress for NC-Cu-10at.%Ta (Figure 3.8) reveals that the upturn in the flow stress is delayed even at elevated temperatures, i.e., up to 473 K, ($0.35T_m$) where phonons are more prominent as compared to the room temperature, and yet, a negligible dependence persists up to strain rates on the order of ~$1.8x10^4$ s^{-1}. In general, we know that the classical quantum mechanical description

predicts the nature of phonons to obey Bose-Einstein statistics [21]; hence, the mean occupancy number of phonons increases linearly with temperature. As the number of phonons increases, drag force on a mobile dislocation also increases leading to a rapid increase in flow stress at low strain rates which becomes apparent when the temperature for NC-Cu-10at.%Ta is increased to $0.64T_m$ (873 K). Further, sufficient thermal energy is now available for dislocations to overcome thermal barriers, such as nanoclusters, which allows dislocations to reach their highest velocity leading to an increase in flow stress due to phonon drag. However, despite increasing the mean occupation of phonons by 3 orders of magnitude (as given by Bose-Einstein statistics [21]), the influence of phonon-drag, i.e., the increase in the normalized flow stress for NC-Cu-10at.%Ta at $0.64T_m$, is similar to that exhibited by coarse grained pure Cu at $0.22T_m$ (298 K). Furthermore, it must be noted that the drag coefficient increases significantly when the material strain rate is increased by a small fraction beyond a critical rate (generally, on the order of 10^3 s^{-1}). For example, as a direct result of a marginal increase in strain rate at 573 K, NC-Cu-10at.%Ta has attained a similar level of normalized flow stress to when tested at 873 K, despite a 300 K difference in temperature. This observation highlights the significance of the minimal increase in normalized flow stress resulting from the Taylor anvil experiments, e.g., deformation at very high strain rates (10^5 s^{-1}). Eventually, the effects of temperature begin to dominate the dislocation phonon interactions and at $0.79T_m$ (1073 K), NC-Cu-10at.%Ta demonstrates a clear upturn, which is indicative of the true non-Arrhenius dependent regime of deformation.

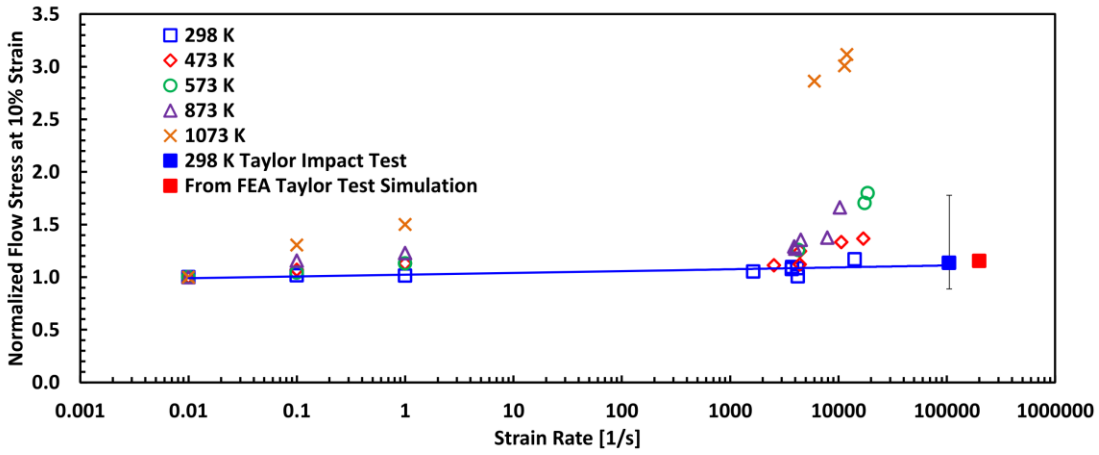

Figure 3.7 Combined thermal and strain rate dependence of the flow stress of NC-Cu-10at.%Ta. NC-Cu-10at.%Ta at varying testing temperatures. Data above 10^5 s^{-1} was approximated using Taylor tests. The solid lines are power law fits for room temperature and 473 K, which indicate that the stable material follows thermal activation processes up to strain rates on the order of 10^5 s^{-1} and temperatures up to 473 K.

The flow stress results for both low and high strain rates reveal an apparent linear temperature dependence [1,12] as compared to the sigmoidal manifestation expected for pure, coarse grained Cu as observed in Figure 3.9. In pure, coarse-grained Cu, the values of the flow stress are a result of thermally activated dislocation motion, where an increase in temperature increases the energy of the dislocation and lowers the activation energy that the dislocation must overcome to propagate. Thus, the flow stress (σ_f) decreases with temperature following an Arrhenius relationship as seen below (also refer to [47]).

$$\sigma_f = Ce^{\frac{-Q}{RT}} \tag{3.1}$$

where C is a constant, Q is the activation energy, R is the ideal gas constant, and T is the temperature. However, for NC-Cu-10at.%Ta, the flow stress is seen to decay near linearly as temperature increases. Moreover, the Cu grain size in NC-Cu-10at.%Ta after

testing at 1073 K (800 °C) was estimated to be about 90 nm [13], indicating that grain coarsening is very limited and the reduction in observed yield and flow stress is solely dependent on increased thermal softening. In other words, the stable microstructure of the NC-Cu-10at.%Ta alloy retains close proximity of dislocation barriers such as grain boundaries and nanoclusters such that these act as short range barriers to dislocation motion [2]. As increased temperature aids in overcoming short range barriers through increasing the vibration of dislocated atoms while long range barriers (e.g., grain boundaries) remain stable, the stress required to further deform the specimen (i.e., flow stress) decreases linearly. Thus, NC-Cu-10at.%Ta exhibits an extremely stable microstructure and unusual mechanical properties.

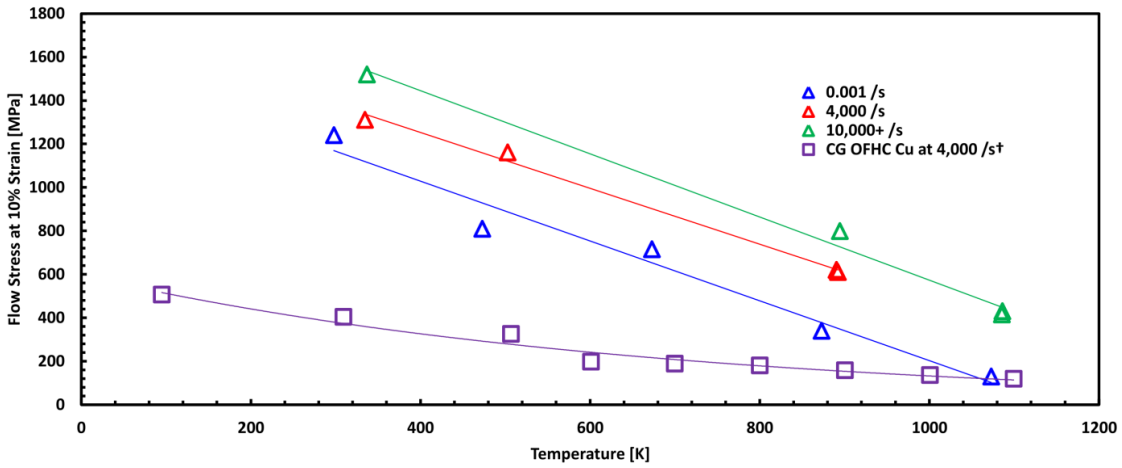

Figure 3.8 The linear behavior of flow stress as a function of temperature for NC-Cu-10at.%Ta**.** The behavior of the NC-Cu-10at.%Ta alloy most closely follows a linear trend as compared to the exponential trend of the OFHC Cu from the data of [64] denoted above with a symbol †.

The plastic deformation in NC-Cu-10at.%Ta tested here was determined to occur either through deformation twinning or dislocation slip. Studies have indicated that GBs

serve as the origin for nucleation and provide a point for storing and annihilating/absorbing dislocations after they transverse the grain under an applied stress. These GBs are also responsible for pinning the dislocations ultimately obstructing their motion by strongly influencing when and where cross-slip can occur and by increasing the energy to unpin and move across to the neighboring grains [43–46]. Quasi-static and high strain rate testing are fundamentally different processes as the time scale of deformation in quasi-static tests is longer than the time for dislocations to form and propagate; whereas, the time for deformation in high strain rate tests is too short to allow dislocation motion to dominate without the influence of dislocation drag. As a result, the plasticity accommodation will be inherently different between quasi-static and high strain rate tests.

To investigate the active deformation mechanisms and the reasoning behind the high temperature and strain rate response in these alloys, ex-situ microstructural characterization was employed using the same techniques employed to investigate the as received microstructure. In general, the emissions of partial and full dislocations are competing mechanisms and their activation depends on the stress level and testing temperature. From the TEM observations presented here on NC-Cu-10at.%Ta, an appreciable dislocation density can be identified for quasi-static testing conditions implying an absence of dislocation absorption. In the case of conventional nanocrystalline materials, grain boundaries act as a source for dislocation generation. The dislocations are then free to traverse the grain and be absorbed at the opposite grain boundary which acts as a sink. In the NC-Cu-10at.%Ta alloy, the dislocations are

emitted, interact with the high density nanoclusters, and become pinned at various sites, thereby, reducing the mean free path for the propagation of the dislocations. Figure 3.10 illustrates the variation in inter-cluster spacing for Ta nanoclusters as a function of strain rate at various testing temperatures. It can be seen that both temperature and deformation rate have minimal influence on the spacing, which confirms the stability of the alloys. The restricted motion of dislocations is the result of an un-pinning stress that the dislocation must overcome for motion to resume. The propensity of dislocation slip increases for both quasi-static and dynamic testing conditions with an increase in testing temperature, which helps in overcoming the energy barrier required for dislocation based activity in these systems. However, the mean free path for the dislocation motion is dependent on the grain size and density of the nanoclusters that are embedded in the material system. In the case of high strain rate conditions, nucleation of partial dislocations is favored at RT due to the high applied stress which surpasses the barrier for twinning based deformation, and further, the growth of the twins is restricted due to the presence of Ta nanoclusters in NC-Cu-10at.%Ta [41] which leads to the nucleation of new twins. However, at elevated temperatures, the deformation shifts from twin based to dislocation based where, again, the thermal energy favors dislocation slip.

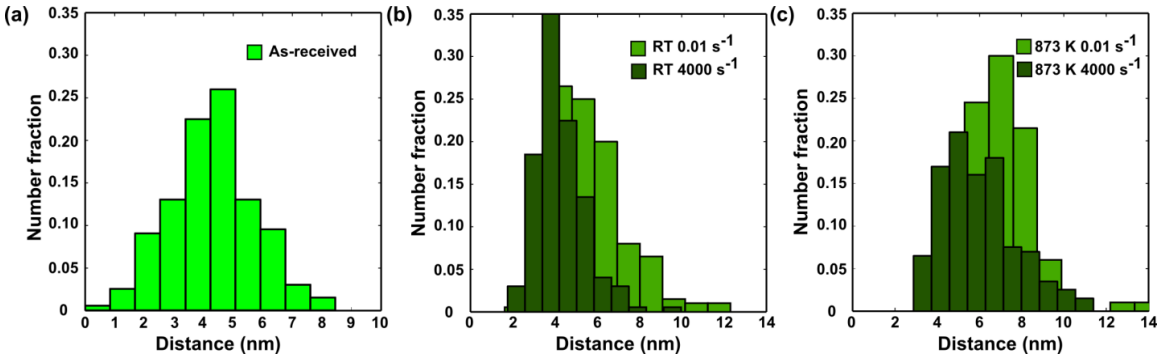

Figure 3.9 Inter-cluster spacing as a function of testing condition. The distributions indicate little or no variation in the average spacing of Ta particles with an increase in temperature or deformation rate reaffirming the stability of the nanoclusters.

3.4 Discussions

As observed in the flow stress response of polycrystalline OFHC Cu, polycrystalline Ta, and NC-Cu as a function of strain rate, the flow stress above ~4×10^3 s^{-1} changes dramatically with a small increment in strain rate. There is debate as to the source of this upturn in flow stress where traditionally, the upturn was believed to be the result of a drag force acting on the dislocations while more recently, some researchers have shown that the increase in flow stress may instead be the result of an increased number of dislocations at these strain rates [63,65]. It could also be proposed that at such high strain rates, the effects of inertia may influence the strain rate at which the upturn in flow stress is observed, but following the method outlined by [14,66] for determining critical strain rates where inertia plays a role, Figure 3.11 shows that while the higher strain rate (> 1.2 x 10^4 s^{-1}) data from Follansbee and Kocks [63] could be influenced by inertia (see also [66]), the results obtained here for NC-Cu-10at.%Ta fall well below the critical strain rate for inertia. Further, Jordan et al. [14], who account for inertia in their data, observe the upturn in flow stress in pure Cu at around 10^3 s^{-1}. In short, Follansbee and Kocks [63]

observe the flow stress upturn at a higher strain rate than Jordan et al. [14] owing to detrimental inertia effects in the data of Follansbee and Kocks. However, here as a result of no inertia effects, the lack of flow stress upturn in NC-Cu-10at.%Ta cannot be explained as a geometric effect and, therefore, must be a real material response.

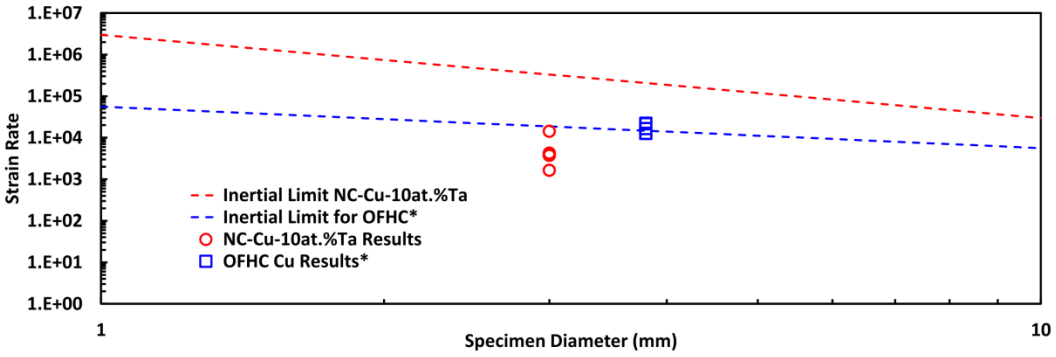

Figure 3.10 Specimen size and strain rates compared to inertial limits for OFHC Cu and NC-Cu-10at.%Ta. While the data from Follansbee and Kocks [63](*) may be influenced by inertia at strain rates above 1.2 x 10^4 s^{-1}, the NC-Cu-10at.%Ta data all fall well below the strain rates where inertia plays a major role indicating that the flow stress is not significantly influenced by inertia effects.

Flow stress measurements taken at constant plastic strain in pure Cu materials indicate an upturn in flow stress likely resulting from the influence of drag forces on mobile dislocations. As stated in chapter 1, the drag force on a mobile dislocation, assuming negligible effects of electron drag and magnon drag, is classically stated to be proportional to the flow stress of the material and determined as below

$$F = B_{ph} v \tag{3.2}$$

where v is the dislocation velocity which is dependent on the strain rate and B_{ph} is the drag coefficient for phonon interaction determined by

$$B_{ph} = \frac{3kT}{b^2 c_s} \tag{3.3}$$

where k is the Boltzmann's constant, T is the temperature of the material, b is the Burger's vector, and c_s is the wavespeed of the material [20]. This would indicate that the effects of phonon drag have the strongest influence at higher temperatures and higher strain rates which is what is observed in Figures 3.6 and 3.8 for pure Cu and for NC-Cu-10at.%Ta at temperatures above 473 K. By contrast, however, dislocation pinning in the NC-Cu-10at.%Ta alloy below 473 K delays the flow stress upturn mechanisms until higher strain rates than found in pure CG and NC Cu.

For general cases, deformation mechanisms are depicted in Cu materials in Figure 3.12. In CG pure Cu, the distance between dislocation barriers relative to the width of the dislocations is large allowing the dislocations to propagate freely. This allows low flow stresses at low strain rates, but in the phonon drag theory, as strain rates increase to the 10^3 s^{-1} regime, the dislocations begin interacting with vibrating atoms within the crystalline lattice. The result is a higher energy barrier that the dislocation must overcome for further propagation. The heightened energy barrier can lead to lower energy deformation mechanisms such as twinning to occur, but as seen by the upturn in flow stress observed for CG pure Cu in Figure 3.6, dislocation motion appears to be the preferred deformation mechanism up to the range of strain rates where the upturn in flow stress is apparent.

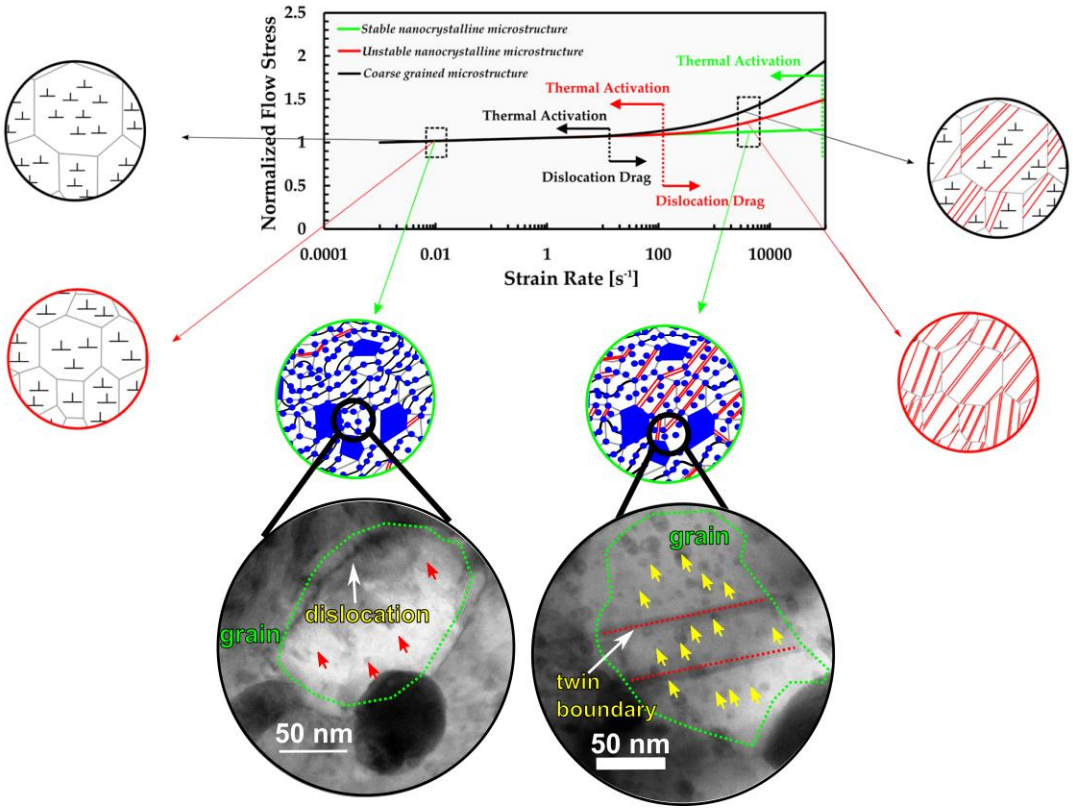

Figure 3.11 Depiction of general mechanisms for CG and NC pure Cu compared with that observed here in NC-Cu-10at.%Ta. All three materials deform primarily by way of dislocation nucleation and propagation at quasi-static strain rates. However, at high strain rates, CG Cu (black circles) will continue to be dominated by dislocation mobility leading to an increased influence of phonon drag; while, NC pure Cu (red circles) will exhibit extensive twin formation and growth leading to grain rotation and growth where the effects of drag dominated plasticity will result from the continued motion of full and partial dislocations. In contrast, nucleating twins are arrested by Ta dispersions and grain boundaries in the NC-Cu-10at.%Ta (green circles and TEM micrographs) at high strain rates causing more twins to nucleate to accommodate plasticity. The nucleation of twins is not affected by drag at strain rates below 10^5 s^{-1} as the partial dislocations are unable to reach an average maximum velocity due to the short spacing between obstacles.

The introduction of barriers, such as grain boundaries and Ta nanoclusters can delay the flow stress upturn by acting as short range barriers to pin the dislocations such that lower energy deformation mechanisms such as twinning become preferable to dislocation motion. However, in the case of NC pure Cu, the nanocrystalline structure is unstable, so

the grain boundaries become less concentrated at high strain rates (resulting from pressure driven grain growth) and high temperatures leading to similar deformation mechanisms seen in the CG pure Cu. In contrast, the stabilization of grain boundaries and introduction of nanoclusters achieved in NC-Cu-10at.%Ta result in a high number of barriers to dislocation motion at both high strain rates and high temperatures. At low strain rates, the deformation of the NC-Cu-10at.%Ta is primarily a result of dislocations overcoming the activation energy imposed by grain boundaries and nanoclusters. As a result, the quasi-static flow stress for NC-Cu-10at.%Ta exceeds the flow stress of CG pure Cu by more than a factor of 5 at a strain rate of 1 (±0.5) x 10^{-1} s^{-1}. However, at room temperature and strain rates above 10^3 s^{-1}, the deformation mechanism shifts from being dislocation dominated to being dominated by twin nucleation. In NC-Cu-10at.%Ta, a high number of narrow twins appear when the alloy is strained at strain rates on the order of 10^3 to 1.8x10^4 s^{-1}. By comparison, twins formed in the pure Cu are expected to be wide implying that they have undergone growth during loading. However, as seen, twin growth is impeded by Ta nanoclusters in the NC-Cu-10at.%Ta alloy. As a result, twin nucleation is preferable (with limited growth or dislocation motion) such that an increase in flow stress is not observed up to strain rates of 1.8x10^4 s^{-1}. With the addition of temperatures exceeding 573 K (300 °C), dislocation slip becomes more dominant as compared to twin nucleation, and the flow stress upturn is observed at strain rates near 1.8x10^4 s^{-1}. A high number of dislocation interactions with Ta based particles appear within grains of NC-Cu-10at.%Ta alloy strained at rates on the order of 10^3 to 10^4 s^{-1} and temperatures > 573 K (300 °C).

Finally, recent atomistic-continuum modeling of phonon drag mechanisms provide further insight into the physics governing the anomalous mechanical behavior observed in NC-Cu-10at.%Ta [22]. Although the modeling results were obtained for "2-D" Cu starting at 0 K, the qualitative behavior should be fairly relevant. Xiong et al. [22] reported that dislocations were found to accelerate rapidly for about 10 ps before reaching a more steady propagation velocity. In 10 ps, the dislocations moved about 20 nm (or about 55 lattice parameters). Given the spacing of the Ta particles (see Figure 3.10), this would suggest that dislocations in NC-Cu-10at.%Ta cannot accelerate to a full steady state before running into an obstacle (Ta nanocluster, about 10-14 lattice parameters apart), thus "jerky" dislocation motion leading to serrated flow, climb and cross-slip are likely resulting in a linear temperature dependency. Thus, the interaction of dislocations with Ta based particles will incur some delayed time relative to free glide during particle bypass reducing the mean velocity and delaying the onset of flow stress upturn. The velocity and density of mobile defects including dislocation or deformation twin generation at a propagating shock front is dependent on the percent strain and strain rate. The constitutive relation is given by the following equations [2].

$$\frac{d\varepsilon}{dt} = \frac{1}{m}\rho b v \quad or \quad \frac{d\varepsilon}{dt} = \frac{1}{m}\left(\frac{d\rho}{dt}\right) b\Delta x_d \tag{3.4}$$

where m is an orientation factor for resolution of the strain tensor, ρ is the dislocation density, expressed in line length per unit volume, v is the average dislocation velocity, $d\rho/dt$ is the rate of dislocation generation and Δx_d is the average distance moved by the dislocations. Here it can be seen that two scenarios arise to explain the observed

behavior. That is, not only is the velocity and average distance traveled by the dislocation during impulse loading relevant but also the nucleation rate. Past findings indicate that high densities of dislocations generated by pre-shocking Cu samples can lead to a delayed upturn of flow stress with strain rate [67] upon reloading. NC-Cu-10at.%Ta alloys do present an increased number of dislocation nucleation sites (grain/twin boundaries and particle interfaces), and Ta particles occupying grain/twin boundary regions can alter the dislocation nucleation rate. The combined effect will ultimately modify the density of mobile dislocations under a given strain rate (as given by Orowan's equation [2]). However, it should be mentioned that such high densities of dislocations, as in the case of [67] are extremely unstable and subject to dynamic crystallization of the microstructure upon reloading, unlike the stabilized microstructure exhibited by stabilized NC-Cu-Ta alloys presented here. Additionally, there comes a point where the dislocation nucleation rate should become damped out due to the balance of the inherent annihilation rate (i.e. saturation) or simply unsustainable in suppressing dislocation velocity with increases in strain rate. Therefore, if the strain rate is high enough, eventually all mobile dislocations, regardless of density, will be accelerated to the shear-wave speed of the specific material.

It should be mentioned that thermodynamically, plastic deformation is an essentially irreversible phenomenon leading to a change in shape, which is not a state function, i.e., the end state is path dependent. That is, the nucleation rates and dislocation densities are not state quantities but rather internal variables. Under high strain rate deformation, the dynamic rearrangement due to application of forces and relaxation of internal variables

are of the same order and the concept of a locally constrained equilibrium state breaks down [68]. Such a process must then be modeled using extended irreversible thermodynamics. Additionally, such variables are extremely difficult to measure and quantify accurately, especially in nanocrystalline metals where grain boundaries are the main sources and sinks. This poses extreme mathematical difficulties and severe limitations to understanding these types of processes with phenomenological or analytical modeling. At this time it is not possible to discern which perspective (velocity or nucleation/distance limited) is more applicable to the actual physics governing the response in NC-Cu-Ta alloys, and more work is needed.

As discussed previously, at elevated temperatures, crystalline-defects (twin boundaries and/or dislocations) that are free to move within the microstructure will interact with a viscous phonon gas (derived from random lattice vibrations) leading to an increase in the drag effect during high-rate deformation. Furthermore, the result of accelerating defect dislocations (full and twin) to dynamic rates is known to produce elastic waves in the form of anharmonic radiation, with a wavelength that is dependent on and proportional to the velocity [22]. However, at finite temperatures, the emitted phonons from dislocations or other sources will be partially absorbed or scattered by the viscous medium of thermal phonons and likely not travel extended distances. The high density of barriers, such as grain/twin boundaries and the high number density ($6.5 \times 10^{23}\ m^{-3}$) of nanoclusters (Figure 3.2) can lead to scattering, absorption and transmission, which should distort the local phonon density of states and produce perturbations in the elastic/plastic front. Such interfaces/defects are known to

significantly influence thermal transport properties [23]. While it is not expected that specific frequencies will be truncated [22], dispersed particles and interfaces will generate, reflect, and absorb phonons differently from the matrix or free surfaces.

Recent findings do confirm that dislocations decelerate when reflected phonon waves from the free surface interact with the moving dislocations leading to a decrease in the driving force and an increase in the drag. In this case, phonons from the Cu lattice will also interact with the Ta nanoclusters and available interfaces such as grain and twin boundaries and partially reflect (and partially transmit), leading most likely to changes in the phonon density of states and altered interactions with dislocations. Furthermore, the results from [22] also showed that phonons emitted by dislocations have wavelengths that depend on their velocity: the faster the dislocation, the longer the wavelength. They observed that most phonons emitted had wavelengths of 5 lattice parameters or more, which is nearly half the inter-nanocluster spacing, i.e., the phonon wavelength is commensurate with the microstructural length scale and phonons should get scattered by the particles, and the lower velocities that dislocations should reach as they run into these nanoclusters should keep long wavelength phonons from developing effectively.

In summary, crystalline-defects (twin boundaries and/or dislocations) at elevated temperatures are free to move within the microstructure and will interact with a viscous phonon gas (derived from random lattice vibrations) leading to an increase in the drag effect during high-rate deformation. Additionally, the result of accelerating defect dislocations (full and twin) to dynamic rates is known to produce elastic waves in the form of anharmonic radiation, with a wavelength that is dependent on and proportional to

the velocity [22]. However, at finite temperatures, the emitted phonons from dislocations or other sources will be partially absorbed or scattered by the viscous medium of thermal phonons and likely not travel extended distances. The high density of barriers, such as grain/twin boundaries and the high number density (6.5×10^{23} m^{-3}) of nanoclusters (Figures 3.2 and 3.3) can lead to scattering, absorption, and transmission, which should distort the local phonon density of states and produce perturbations in the elastic/plastic front. Such interfaces/defects are known to significantly influence thermal transport properties [23]. Recently, some atomistic studies showed that decreasing grain sizes in pure NC metals enhances both the low and high frequency phonon density of states (DOS) [22]. These works showed that the lower atomic density in grain boundary regions enhances the low-frequency vibrational modes as well as promotes general broadening of the phonon DOS due to disorder; whereas, the internal stresses within the NC grains shift the phonon DOS to higher frequency [22]. Alternatively, and in addition to contributing to the scattering and absorption of phonons, boundaries and nanoclusters can delay the transition to the drag regime by acting as barriers that pin and slow down defect propagation.

In conventional NC metals such as pure Cu, the defects, i.e., grain/twin boundaries, are unstable with respect to temperature and stress/pressure [69], so the grain/twin boundaries become less concentrated under the conditions tested here, leading to increased phonon effects on the flow stress response. However, in NC-Cu-10at.%Ta at room temperature, Figure 3.12 illustrates pinning of partial dislocations by stable nanoclusters and grain boundaries. Additionally, Ta nanoclusters, with average

dislocation pinning distance of ~5 nm, contribute to effectively negate the influence of phonons even at high temperatures where they are seen to interact with and pin dislocations/networks.

Based on the constitutive relation governing strain rate, the mean mobile dislocation velocity, distance translated, nucleation rate, and density play important roles in defining flow stress [47]. In simulations of Cu, it was reported that dislocations were found to accelerate rapidly for about 10 picoseconds before reaching a more steady propagation velocity [22]. In 10 picoseconds, the dislocations moved about 20 nm (or about 55 lattice parameters). Given the spacing of the nanoclusters, this would suggest that dislocations in NC-Cu-10at.%Ta cannot accelerate to a full steady state before running into an obstacle. Furthermore, the average steady state velocity will decrease as some delay in time will occur during particle bypass with the magnitude of this waiting time being dependent on the temperature particle matrix coherency. As the sample is continuously deformed at elevated temperatures, both the dislocation density as well as the nucleation rate should change. However, these mechanisms, nucleating and storing/transmitting dislocations, will inevitably be altered by the presence of the dense nanocluster network within boundary and inter-crystalline regions. What does seem apparent from the elevated temperature data and micrographs is that, with an increase in temperature, more dislocations and fewer twins are observed. It is likely that high temperatures reduce the time delay for particle bypass in NC-Cu-10at.%Ta through thermal activation, allowing the dislocations to translate more freely with a higher average velocity incurring increased phonon-drag.

3.5 Conclusion

The present study shows that when the material microstructural length is reduced to an extremely fine grain size (in the nanocrystalline regime); the flow stress remains relatively insensitive to the increase in the rate of deformation (up to 10^5 s^{-1}). This is in part due to the influence of a high concentration of stable defects (interfaces and particles) which alter the phonon DOS through generation, scattering, and absorption as well as the average dislocation velocity, distance traveled, and likely the nucleation rate and density preventing/delaying phonon drag until much higher strain rates than normally observed in currently known systems. In general, the implications of such observations place NC among the strongest, most resilient, and most thermally stable known structural materials; hence, there is potential in designing new, tougher materials for advanced applications, such as those from power generation-reliant industries, low temperature (cryogenic) applications, and space shielding (unique spall-fragmentation behavior). Overall, we have shown, for the first time, that phonon-drag effects in stable nanocrystalline materials diverge from the conventional understanding, and the strain rate that marks the onset of the transition to the phonon-drag regime can, at the very least, be delayed to higher strain rates, thus providing a clear path for designing materials for low temperature as well as extreme strain rate applications.

4 TENSILE BEHAVIOR OF A NANOCRYSTALLINE/ULTRA-FINE GRAINED ALLOY UNDER VARIABLE PROCESSING CONDITIONS

The interplay between the microstructure of a powder processed Cu-Ta alloy and the strain rate at which flow stress upturn occurs is investigated. Varying Ta concentration and processing temperature allows investigation of varied Ta dispersions with the grains as well as differing grain sizes ranging from the nanocrystalline to the ultrafine grained regimes. Results show that nanocrystalline material exhibits brittle behavior at low strain rate but increased ductility at high strain rate which is opposite to observations in the ultrafine grained material. Further, as grain size increases and Ta concentration decreases, flow stress upturn is observed at lower strain rates.

4.1 Introduction

The promise of excellent mechanical strength and ductility without additional weight makes nanocrystalline materials highly desirable in applications such as vehicle structures and armor plating, but nanocrystalline materials are plagued by unstable structures causing them to lose these exceptional properties under extreme environmental conditions such as high temperatures and high loading rates. Reviews by Koch and Andrievski [6,8] provide insight into the current state of the art regarding nanocrystalline processing and mechanical behavior, and both mention the problem of stability of a nanocrystalline structure under both thermal and mechanical loads. Using an electrodeposited Al thin film which was shown to exhibit no room temperature grain growth, Rupert et al. [69] studied the effect of mechanical load on grain growth and

found that stress driven grain growth was significant in unstable nanocrystalline materials. This result is supported by results from Gianola et al. [70] who further proposed that a number of factors such as initial specimen texture, grain boundary energy, and solute pinning have major effects on either facilitating or stabilizing grain growth. In fact, most of the above papers have mentioned the stabilizing effect of drag forces on the grain boundaries caused by solutes forming at the grain boundaries. Therefore, the addition of impurities allows the possibility of tailoring the stability of the microstructure such that mechanical properties unique to nanocrystalline materials can be probed without a loss of nano-structure.

Nanocrystalline instability complicates understanding the fundamental effect of nanocrystalline grain size on the mechanical behavior of this class of materials. For example, Dalla Torre et al. [18] show that NC pure Ni, which is unstable during high strain rate loading, exhibits significant strain rate sensitive flow stress at strain rates that are lower than those at which coarse grained pure Ni observes noticeable strain rate sensitivity (see Figure 1.3). However, chapter 3 shows that a stable nanocrystalline material, NC-Cu-10at.%Ta which has both nanocrystalline grain size and finely dispersed Ta particles, exhibits no upturn in flow stress up to strain rates of 10^5 s^{-1}. In this work, the separate effects of grain size and Ta dispersions are analyzed in order to guide efforts in developing optimizable alloy systems for delayed flow stress upturn.

4.2 Materials and Methods

In an effort to distinguish between the effects of grain boundaries and Ta dispersions on the strain rate at which flow stress upturn occurs, three different compositions of a Cu-Ta alloy, namely Cu-1at.%Ta, Cu-5at.%Ta, and Cu-10at.%Ta were synthesized using procedures similar to those outlined in chapter 2, but with varying processing temperatures of 700 °C, 900 °C, and 1000 °C. By varying compositions at similar processing temperatures, the effects of Ta dispersions can be investigated with limited influence from differences in grain size; whereas, varying processing temperatures allow analysis of the effects of grain size with limited influence of varying Ta dispersions.

Samples for tensile testing were cut along the extrusion direction of the billets in the form of rectangular dogbone specimens as shown in Figure 4.1a. Rectangular cross-section specimens do not provide an accurate measure of flow stress within the plastic regime of deformation due to inertial effects causing stress concentrations near the corners, but they are useful in measuring the yield stress of the material which is taken here to be equivalent to the flow stress at a 0.2% offset in the plastic strain. Quasi-static tensile tests at 10^{-3} s^{-1} are performed with an electromechanical universal testing machine equipped with an extensometer and corrected to reveal true stress-true strain results. High strain rate tests are conducted using the Kolsky bar technique described in [26,71] but with specialized grips to accommodate the rectangular dogbone specimens. The strain rates of Kolsky bar testing in this work are around 5×10^{3} s^{-1}, and samples are strained until failure.

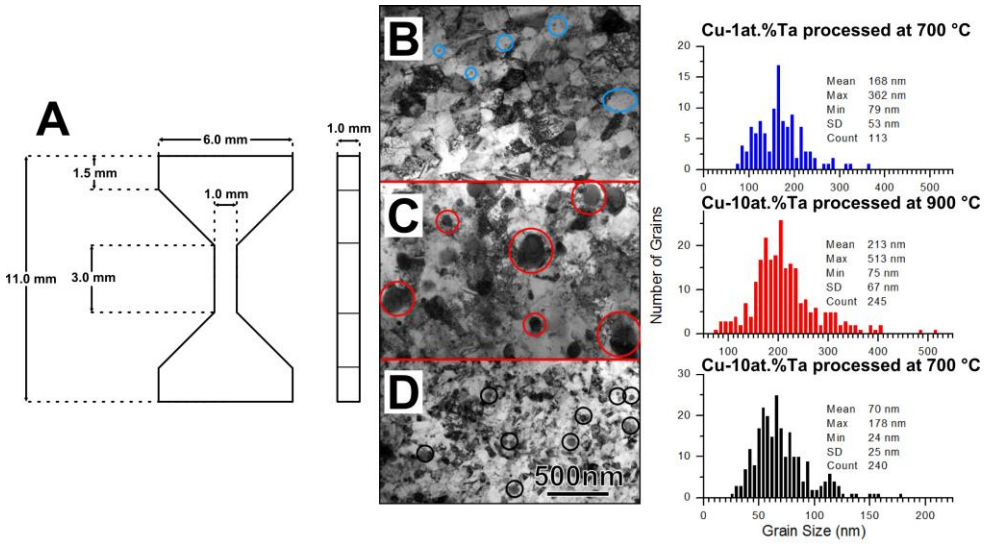

Figure 4.1 a) Rectangular dogbone tensile specimen dimensions and b-d) TEM micrographs and grain size statistics for the Cu-1at.%Ta processed at 700 °C, Cu-10at.%Ta processed at 900 °C, and Cu-10at.%Ta processed at 700 °C, respectively. Microstructure images and statistics come from [2].

4.3 Results and Discussions

In the results from chapter 3, the stable nanocrystalline structure of Cu-10at.%Ta processed at 700 °C, which possessed nanocrystalline structure along with a high number of Ta nano-dispersions, exhibited no flow stress upturn up to strain rates of 10^5 s^{-1} during compression loading. It can be reasonably assumed that as processing temperature is increased, the grain size of the alloy also increases and the Ta nano-dispersions become more dispersed. Further, with a reduced Ta concentration, fewer Ta dispersions are available to pin grain boundaries, so some grain growth should be observed for samples processed at similar temperatures but with lower Ta concentration; however, the grain growth is expected to remain low compared to the growth observed from raising the processing temperature (e.g., Cu-1at.%Ta processed at 700 °C should experience less grain growth than Cu-10at.%Ta processed at 900 °C). The TEM images of Figure 4.1

reveal that the Cu-10at.%Ta processed at 700 °C has truly nanocrystalline structure (average grain size less than 100 nm) while the other alloys fall within the ultrafine grained regime (average grain size between 100 and 1,000 nm). The TEM analysis for Cu-5at.%Ta processed at 700 °C is currently still in progress, but the structure is assumed nanocrystalline based on the nearly nanocrystalline structure of the Cu-1at.%Ta processed at 700 °C.

Tensile testing results in Figure 4.2 reveal a unique distinction between the nanocrystalline samples and the ultrafine grained specimens. Namely, at quasi-static strain rates, the samples processed at 700 °C, i.e., the samples with the smallest grain size, exhibit limited ductility while the larger grained samples experience ductility between approximately 5% and 10%. Further, at high strain rates, the larger grained samples experience higher flow stress and lower ductility than observed at quasi-static strain rate as would be expected in a typical high strain rate test of a polycrystalline sample; however, the samples processed at 700 °C experience increased ductility along with increased flow stress at the higher strain rates. This increase in ductility is likely a result of a mechanism shift from dislocation propagation and absorption to twin nucleation as observed under compression in chapter 3 which was held to be the cause for the lack of flow stress upturn under compressive load.

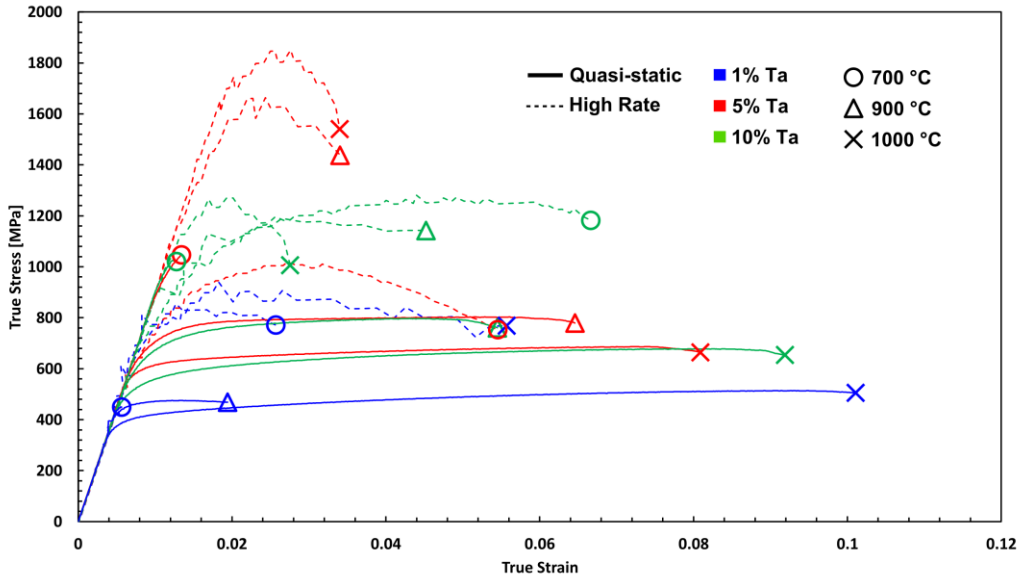

Figure 4.2 Tensile stress-strain results for the various samples at both quasi-static and high strain rates.

Further, observations of flow stress in Figure 4.2 reveal a significant increase in flow stress at high strain rate for samples with larger grain size and lower Ta concentration. Table 4.1 lists the resultant yield stresses (failure stress in the case of Cu-10at.%Ta and Cu-5at.%Ta processed at 700 °C) for each specimen which are also shown compared to compression results for Cu-10at.%Ta processed at 700 °C from chapter 3 in Figure 4.3. The high strain rate yield stress is normalized by the yield stress at quasi-static strain rate for the same material, so the normalized flow stress is a measure of how much increase in yield stress is observed as a result of the higher strain rate of deformation. Specimen results are listed in order from lowest normalized yield stress to highest normalized yield stress which allows comparison of initial microstructures shown in Figure 4.1 to the strain rate sensitivity of the material. The results reveal that material with both nanocrystalline grain size and moderate to high Ta concentrations exhibit the lowest rise

in flow stress as strain rate is increased. Further, for each concentration, as processing temperature increases causing grain size to increase, the normalized flow stress also increases. This indicates the importance of grain boundaries in limiting the effects of dislocation drag. Interestingly, though Cu-10at.%Ta processed at 900 °C has a slightly higher grain size than the Cu-1at.%Ta processed at 700 °C, the rise in flow stress was greater for the Cu-1at.%Ta processed at 700 °C indicating that precipitate dispersion also plays an important role in limiting the effects of dislocation drag. This is also seen in the samples processed at 900 °C and 1000 °C where the samples with higher Ta concentration have a lower increase in yield stress than those with lower concentrations of Ta.

Table 4.1 Tensile flow stress results for each sample. Samples are listed in order of their normalized flow stress from lowest to highest.

	Strain Rate	Yield Stress	Normalized Yield Stress
Cu 5% Ta at 700 C	0.001	1046	-
	4990	780	0.745697897
Cu 10% Ta at 700 C	0.001	1024	-
	4100	900	0.87890625
Cu 10% Ta at 900 C	0.001	645	-
	5500	925	1.434108527
Cu 1% Ta at 700 C	0.001	450	-
	4950	760	1.688888889
Cu 1% Ta at 1000 C	0.001	390	-
	6300	770	1.974358974
Cu 5% Ta at 900 C	0.001	700	-
	5500	1565	2.235714286
Cu 10% Ta at 1000 C	0.001	530	-
	4500	1185	2.235849057
Cu 5% Ta at 1000 C	0.001	600	-
	4200	1755	2.925

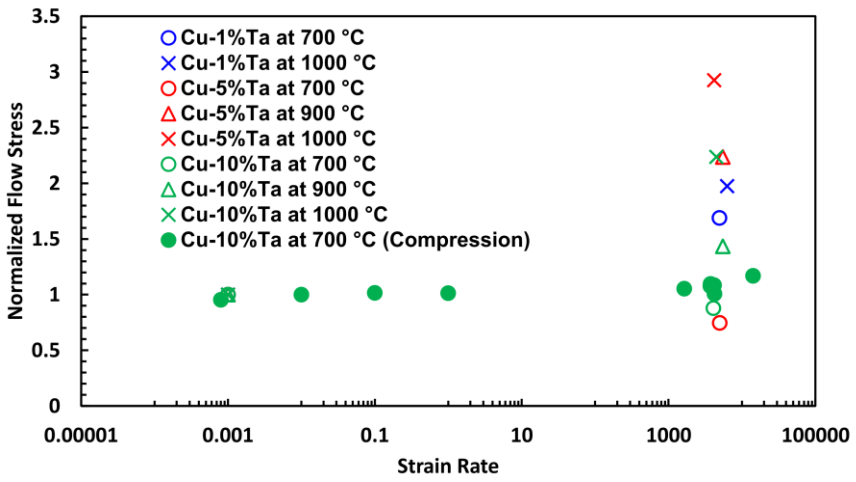

Figure 4.3 Normalized flow stress as a function of strain rate for all samples tested. The data here is compared to compression results found in chapter 3 to clarify the extent of rise in flow stress found in the samples with larger grain size and lower Ta concentration.

The upturn in flow stress resulting from phonon drag can be delayed if dislocations are prevented from reaching a maximum average velocity by delaying the dislocations at defects such as grain boundaries or particle inclusions. Here, nanocrystalline materials with many grain boundaries and many Ta nano-dispersions act as the barriers to these dislocations thus keeping the flow stress within the range of thermal activation processes (i.e., nucleation and propagation of dislocations and twins). Further, interfacial boundaries, as found in grain boundaries and between Cu and Ta phases, complicate the phonon density of states by phonon scattering, transmission, and absorption. As dislocations travel through the spaces between barriers, this complication of the density of phonons may act to limit the phonons through which the sample must travel as compared to the high density of phonons observed in coarse grained, pure material under the same loading conditions (see chapter 3).

4.4 Conclusions

In summary, varying the compositions and processing temperatures of the Cu-Ta system allows investigation of the separate effects of grain size and Ta particle distribution on the flow stress-strain rate response of the alloy. Increasing the processing temperature above 700 °C was found to increase the grain size from the nanocrystalline regime for concentrations of 5at.% and 10at.% Ta into the ultrafine grained regime. Decreasing Ta concentration to 1at.% also allowed grain growth at 700 °C into the ultrafine grained regime, but the effect was less significant than an increase in processing temperature to 900 °C for the 5at.% and 10at.% materials. This shift from the nanocrystalline to the ultrafine grain regime is seen to be sufficient to cause the material to shift from a brittle failure to possessing a ductility of at least 4.5% plastic strain. Further, the nanocrystalline material showed an increase of ductility at high strain rates unlike the decrease in ductility observed in the ultrafine grained materials at high rates. This, combined with previous work (see chapter 3), leads to a conclusion that deformation mechanism changes at high strain rates from dislocation mediated plasticity to twin induced deformation. Finally, a comparison of the change of flow stress at high strain rate relative to that at low strain rate, reveals that a significant rise in flow stress resulting from the interactions of dislocations with lattice phonons is not observed in nanocrystalline materials, but as grain size increases and Ta concentration reduces, the upturn in flow stress appears to occur at lower strain rates. The greater of these effects appears to be the influence of grain size; however, Ta concentrations do play an important role in delaying the onset of phonon drag to higher strain rates.

5 NOVEL KOLSKY BAR TECHNIQUE FOR MEASURING THE DYNAMIC BAUSCHINGER EFFECT IN MATERIALS

The application of a preload on a structural member is known to cause a change in the mechanical behavior of certain materials due to microstructural changes, but when the strain rate of deformation is increased beyond 10^3 s^{-1}, the deformation mechanisms can vary drastically from the mechanisms at low strain rates leading to unique mechanical behavior upon load reversal at high strain rate. In this work, a novel testing technique which allows load reversal at equivalent dynamic strain rates within a few milliseconds of forward loading is outlined, and results for dynamic Bauschinger testing of a low melting temperature alloy (6061-T6) and a stable nanocrystalline structure (NC-Cu-10at.%Ta) are analyzed. For the 6061-T6 alloy, varying strain levels and delay times are utilized to verify the capability of the modified Kolsky bar and analyze the impact of these parameters on the Bauschinger effect in the material. For NC-Cu-10at.%Ta, a compression followed by tension test is performed and compared to separate dynamic compression and tension tests with no preload. Results show that high strain rate loading generates a more substantial difference between forward and reverse flow stress as compared to low strain rate loading in the 6061-T6 alloy. Further, the increased flow stress difference is more exaggerated when the delay time between forward and reverse loading allows specimen recovery as adiabatic heating in the case with no recovery causes softening of the reversed flow stress. Increasing the forward strain level is shown to increase the flow stress difference between forward and reverse loading but more so for the case of no specimen recovery than for the case where the specimen was allowed

time to recover from forward loading. Finally, the dynamic Bauschinger test of NC-Cu-10at.%Ta reveals no significant change in flow stress anisotropy as compared to the separately tested compression and tension results despite expectations that the microstructure experiences extensive twinning during forward loading.

5.1 Introduction

Material mechanical properties are well established for a wide range of materials; however, these properties only explain the performance of the material subject to certain loading conditions such as uniaxial load, low strain rates, and isentropic environments. In practical application, structural materials experience complicated loading environment conditions such as high strain rates, multi-directional loading states, and adiabatic thermal conditions. In particular, load reversal can cause a dramatic change in mechanical behavior due to microstructural changes during the original loading. This, known as the Bauschinger effect [72], has been well studied in many material systems at low strain rates [73–76]. For example, Paul et al. [73] studied the effects of a forward compressive load on the mechanical response of a Ti-Al alloy later pulled in tension. The high number of dislocations and internal stresses formed by compression led to a decreased yield stress upon load reversal. Similarly, Rajagopalan et al. [74] studied the effects of tensile load and unload in nanocrystalline films and found that microstructural heterogeneity arising from varied grain size plays a significant role in increasing the Bauschinger effect in a nanocrystalline material. Haouaoui et al. [75] determined that dislocation tangles in ultra-fine grained Cu cause a backstress which facilitates flow upon load reversal leading to a decreased flow stress. These findings indicate that microstructure, particularly relating to

dislocation formation, plays an important role in anisotropic flow stress behavior resulting from a reversed loading state. Jordon et al. [76] took analysis of the Bauschinger effect in aluminum alloys a step further by analyzing the effect of damage from prior tensile loading on the flow stress of compressed aluminum alloy specimens. They found that accounting for damage allows increased accuracy in prediction of the Bauschinger effect of cast and wrought aluminum alloys. They also found that as the forward strain increases, the reverse flow stress increases for the cast alloy but decreases for the wrought alloy. This indicates that certain microstructural features play unique roles in altering the reversal flow stress, but the specific influence of each microstructural effect is still unclear. To determine the influence of specific microstructural features, significant testing will be required under complicated loading environments.

One such complicated loading environment that would provide insight into the effects of certain microstructural features on the Bauschinger effect is that of loads applied at high strain rates. This insight comes from the high energy and short time scale of deformation during high strain rate testing (above 10^2 s^{-1}) resulting in adiabatic heating and, in some materials, unique microstructural change not observed at quasi-static strain rates (see chapter 3). Adiabatic heating occurs when the plastic work performed on a sample is converted to heat. At quasi-static strain rates, this heat is quickly dissipated to the environment such that the test remains isothermal, but at high strain rates, the time for deformation is too short for heat to be lost. The result is adiabatic temperature rise during the test following the form

$$\Delta T(\varepsilon) = \frac{\int_0^{\varepsilon} \sigma(\varepsilon) d\varepsilon}{\rho C_V} \tag{5.1}$$

where $\int_0^{\varepsilon} \sigma(\varepsilon) d\varepsilon$ is the work performed on the sample due to plastic deformation, ρ is the density of the sample, and C_V is the specific heat capacity at constant volume of the sample [28]. This thermal rise, averaged over the entire specimen, will be lost if the specimen is allowed to recover after forward loading. If the sample is insulated from the Kolsky bar such that no losses occur as a result of conduction, all losses will result from convection and radiation to the environment. Assuming radiation losses are negligible, the thermal loss due to convection is described as a function of time by

$$\Delta T_{loss} = \frac{h_c A \Delta T t_d}{C_V m} \tag{5.2}$$

where h_c is a convection constant (10 $^{W}/_{Km^2}$ for still air), A is the surface area of the sample, ΔT is the temperature rise due to adiabatic heating, t_d is the time allowed for specimen recovery, and m is the mass of the specimen. With this equation, a 6061-T6 aluminum alloy cylinder with Length and diameter of 3 mm, reasonable dimensions for a Kolsky bar specimen, loses all of the heat from adiabatic heating after approximately 0.18 s.

To date, only limited research has been performed to analyze the Bauschinger effect in materials at high strain rates. Dynamic Bauschinger testing has thus far been limited by testing techniques as appropriately timed loading with equal forward and reversed strain rates is complicated. Early work by Nevill and Myers [77] used drop load testing to apply

a preload in high purity aluminum followed by drop load testing in a reversed direction. Their results show that negligible changes in Bauschinger strain parameter were observed as strain rate increased when tensile load was applied first, but when compressive load was applied first, the Bauschinger strain parameter at strain rates above 10^2 s^{-1} increased indicating a lower tensile flow stress. However, as Nevill and Myers point out, samples were allowed to recover from any time dependent effects from preloading such as adiabatic heating. In an effort to limit the time for specimen recovery, Peirs et al. [78] developed a torsional Kolsky bar which allowed reflection of a torsional wave such that the first and second torsional waves impacted the specimen in opposing directions. By comparing with quasi-static results, they showed that the torsional Bauschinger effect in Ti-6Al-4V is strain rate dependent. Similarly, Nemat-Nasser et al. [79] used momentum trapping techniques to reverse a uniaxial Kolsky pulse to allow immediate reversal of the strain, but this technique has been shown to have a difference in strain rates between forward and reversed loading of around 10^3 s^{-1} which is significant for certain strain rate sensitive materials [80].

In this work, a novel procedure for applying equivalent strain rate forward and reverse loads to a specimen at strain rates above 10^3 s^{-1} is explained. 6061-T6 aluminum alloy and nanocrystalline (NC) Cu-10at.%Ta specimens are tested to analyze both the capability of the new device and examine the strain rate sensitivity of the Bauschinger effect including the influence of adiabatic heating in a low melting temperature and stable nanocrystalline material.

5.2 Modified Kolsky Bar

The dynamic Bauschinger testing device is based off of the Kolsky bar, sometimes referred to as a split Hopkinson pressure bar, as outlined in [26] and detailed here in Chapter 1. This technique can be used in compression by firing a solid rod toward the specimen or in tension by firing a hollow tube away from the specimen toward a flange on the incident bar. Here, in order to apply both compression and tension on the same specimen, a compressive pulse was applied on one end of the Kolsky bar assembly and a tensile pulse applied to the opposite end as seen in Figure 5.1. The strikers are propelled by the sudden release of compressed nitrogen gas. The gas is released by simultaneously opening two solenoid valves connected in a parallel circuit. The relative times at which the compressive and tensile waves impact the specimen can be controlled by the spacing of the starting points for the tensile and compressive strikers relative to the points at which the strikers impact the respective incident bars, i.e., if the tensile pulse is to impact the specimen first, the distance between the tensile striker starting position and the incident flange should be shorter than the distance between the compressive striker starting point and the incident bar on the compressive end.

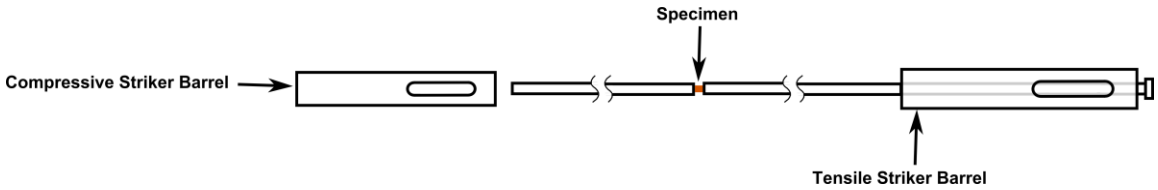

Figure 5.1 Diagram of the modified Kolsky bar.

A Lagrangian diagram which assumes compression immediately followed by tension with 0 s delay time is shown in Figure 5.2. Here, it can be seen that no wave interference

occurs at either the specimen or the strain gauge locations which is necessary for the purpose of obtaining useful measurements from the dynamic Bauschinger test. A representative output from a test for which a delay of 2.5 ms occurred can be found in Figure 5.3. Following such a test, strain gauge signals for tension and compression are analyzed separately using the methods outlined in [26] and combined post processing assuming purely elastic unloading to show the flow stress profile of Figure 5.3b.

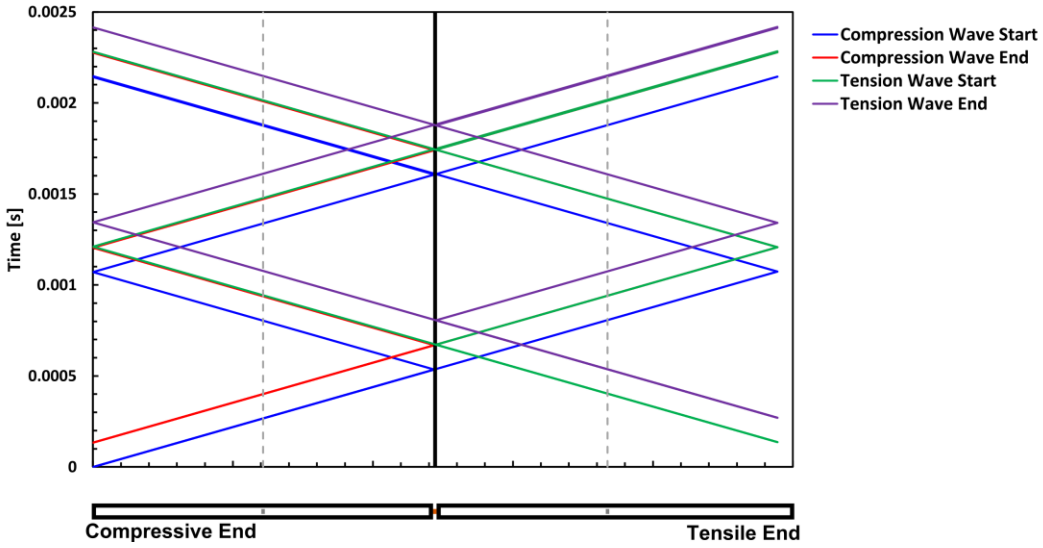

Figure 5.2 Langrangian diagram indicating the position of the waves as a function of time. The dashed vertical lines indicate the position of strain gauge rosettes for measurement of the strain pulses.

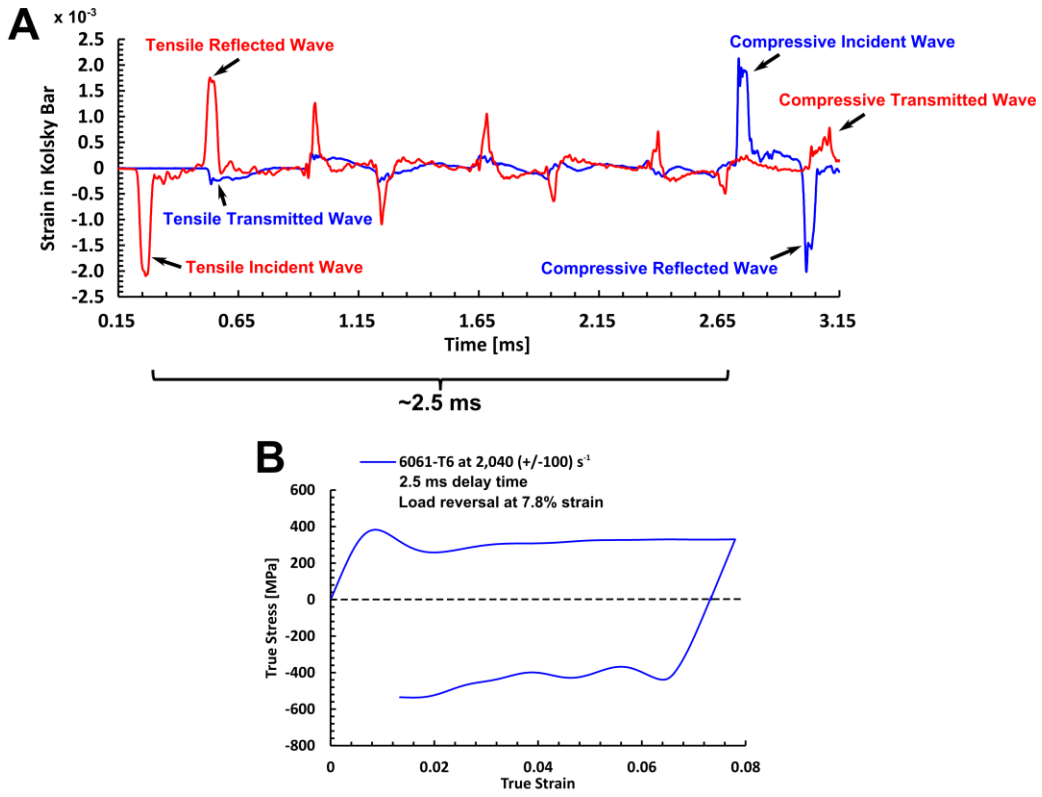

Figure 5.3 Typical results from a dynamic Bauschinger test using the technique outlined in this work. a) Strain signals from the Kolsky bar show that tensile preload can easily be distinguished from a compressive load which follows within 2.5 ms. b) Following data analysis, typical results from the strain signals in (a) are plotted to show the Bauschinger response of the sample. Unloading curves are not measured, so a correction is applied assuming perfectly elastic unloading.

The limit of forward strain is achieved using momentum traps similar to those described by Nemat-Nasser et al. [79], but the momentum traps are equal in mass to the incident bar which they are intended to impact. Spacing between the momentum trap and the incident bar is directly related to the engineering strain observed by the specimen during forward loading and can thus be calibrated. Rough calibration will require the use of at least nine specimens. The more specimens used for the calibration, however, the more consistently can comparable strain rates and strain levels be obtained. Specimens for calibration do not need to be exactly the same as specimens to be tested; however,

specimens with similar impedance are recommended. In order to calibrate the strain rate of deformation, a careful record must be kept of gas gun pressures. As the strain rate within the specimen is dependent on the specimen length, calibration is better achieved using the rate of deformation within the specimen.

$$v_d = 2c_0\varepsilon_r(t) \tag{5.3}$$

Multiplying the desired strain rate by the specimen gauge length and plugging into a fit obtained from previous tests provides the pressure required to obtain the desired strain rate. This calibration procedure should be performed separately for both tension and compression as the gas gun systems will be different due to inherent losses in each system. An example of strain rate calibration is shown in Figure 5.4a. In this case where pressures were kept well within the limits of the gas gun pressure range, a linear fit was preferred, but as the limits of the gas gun are reached, a linear fit may not be preferred. In this case, for a sample of 3 mm gauge length, a strain rate of 5,000 s^{-1} will require a specimen deformation velocity of 15 m/s. Plugging this velocity into y in the equation of Figure 5.4a the gas gun pressure required to achieve a 5,000 s^{-1} strain rate is approximately 142 psi.

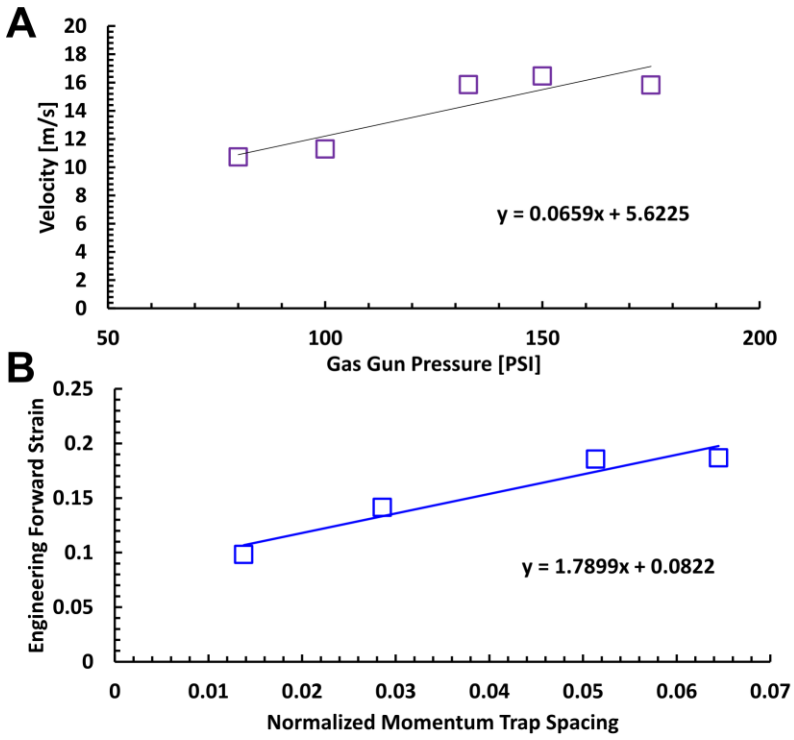

Figure 5.4 a) Calibration of specimen deformation velocity with gas gun pressure, and b) calibration of engineering forward strain with momentum trap spacing normalized by the specimen gauge length.

For calibration of the momentum trap spacing, a record of the spacing between the incident bar and the momentum trap as well as the initial specimen length and final engineering strain is required. In a similar manner to that of the strain rate calibration, the momentum trap spacing is normalized by the specimen length and compared with the forward engineering strain. As seen in Figure 5.4b, the resultant fit provides an estimate for the strain achieved for a given momentum trap spacing. After calibration, tests for 6061-T6 aluminum specimens could be consistently run with forward and reverse strain rates differing by less than +/- 300 s^{-1} and up to strain levels controllable to within +/- 0.2%.

5.3 Results with 6061-T6

Typical results from 6061-T6 aluminum alloy specimens are shown in Figure 5.5. In order to understand the benefits of dynamic Bauschinger testing with nearly no delay time, comparisons are made using samples tested at quasi-static and high strain rates both with specimen recovery and without specimen recovery. Further, the effects of increased reversal strain on the dynamic Bauschinger effect are analyzed using strain levels ranging from 5% to 8% forward strain. From Figure 5.5, it can be seen that significant softening relating to adiabatic heating is apparent during forward loading, but the reversal flow stress does not experience as dramatic a difference in flow stress difference; however, there is sufficient difference between tests to discuss trends in the Bauschinger stress parameter (BSP). The BSP is calculated as

$$BSP = \frac{|\sigma_f| - |\sigma_r|}{|\sigma_f|} \tag{5.4}$$

where σ_f is the forward flow stress (tension in this case) and σ_r is the reverse flow stress (compression here). As samples in a Kolsky test suffer from inertia effects in the early stages of testing, flow stress data is taken at 2.5% plastic strain where force equilibrium was achieved in the sample at both forward and reversed loading. Resultant BSP values for each test were taken and average BSP values are plotted in Figure 5.6 where the error bars represent the maximum and minimum values for all tests run with and without recovery as appropriate. Samples with load reversed within the span of 0.18 s are considered as non-recovered samples. Tensile preload at quasi-static rates causes an increase in the compressive flow stress such that the BSP becomes negative. One

possibility for the increase in flow stress is the onset of damage in the form of void nucleation as mentioned by Jordon et al. [76]. In this case, voids form barriers to plastic deformation during compressive loading. These barriers combine with existing barriers such as precipitates and grain boundaries to cause an apparent compressive strengthening. Further, strain hardening likely plays a major role in deformation of the aluminum alloy as existing dislocations from forward loading may interact with dislocations generated by a compressive load leading to further strengthening. Interestingly, as strain rates increase, regardless of the delay time between forward and reversed loading, the BSP becomes more negative, i.e., the compressive (reversed) flow stress becomes much greater. There is wide variability in the results obtained with no recovery, but the average BSP for specimens with no recovery has a noticeably lower magnitude than the average BSP of specimens which were allowed to recover from adiabatic effects. The lower compressive flow stress of the non-recovered specimens could be explained by the higher testing temperatures resulting from adiabatic heating, but the average temperature before reversed load of each specimen tested without recovery, estimated based on equations 5.1 and 5.2, is 306.5 K which is only 8.5 K higher than the ambient temperature. However, this measure of adiabatic heating is averaged over the entire sample. The possibility of localized adiabatic heating leading to shear band formation has been reported in 6061-T6 aluminum [81] which along with dislocation accumulation during forward loading could also serve to explain the noticeable drop in reversed flow stress at high strain rates.

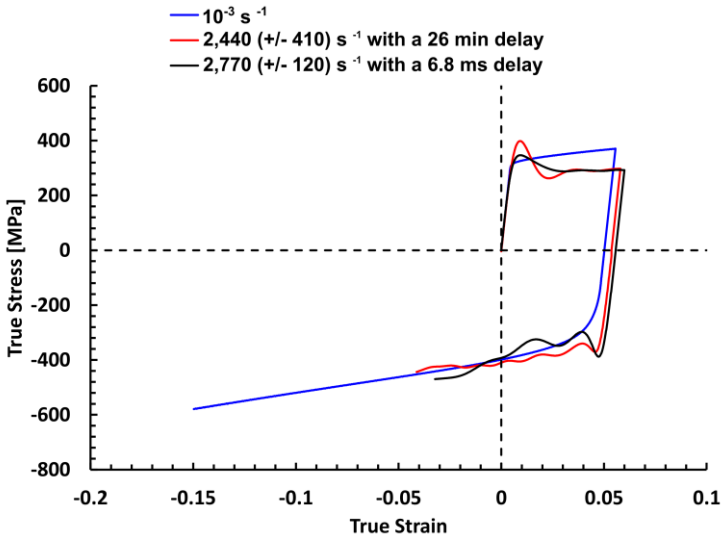

Figure 5.5 Bauschinger plots from select 6061-T6 samples. Parameters for these tests are controlled such that direct comparisons can be made. The strain rates all fall around 2,600 s^{-1} and strain levels are nearly 5%.

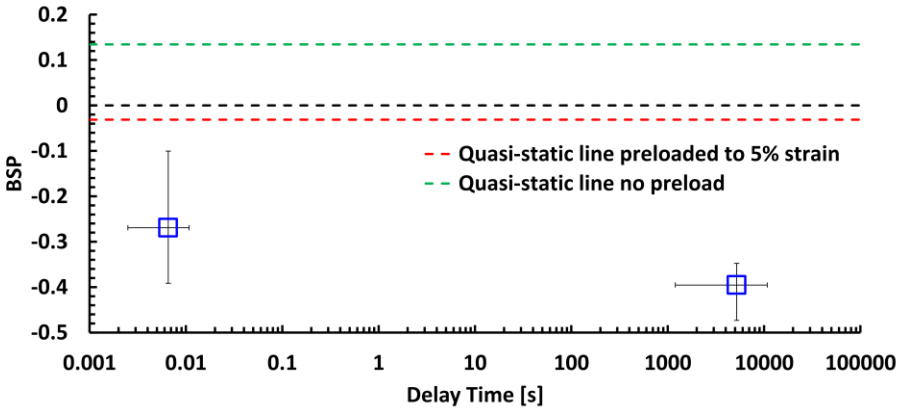

Figure 5.6 Average BSP values for high strain rate tests as a function of delay time compared to BSP values for quasi-static tests both with a tensile preload and without a preload.

Another interesting result is apparent when the BSP is plotted as a function of the strain level at which the load is reversed (Figure 5.7). Here it can be seen that as the reversal strain is increased, the compressive flow stress increases likely as a result of more extensive work hardening and damage. However, in the case of the non-recovered

specimens, the increase in flow stress is more dramatic than that seen in the specimens in which recovery was allowed. Perhaps the increase in thermal energy facilitates the nucleation of a greater number of dislocations leading to greater work hardening, or possibly, shear band interactions lead to strengthening within the material. Further work is required to analyze the morphology of the microstructure and damage state in order to truly understand the mechanism change, but it is evident that the Bauschinger effect is not only strain rate dependent, but also dependent on the strain level and degree of recovery of the specimen after forward loading.

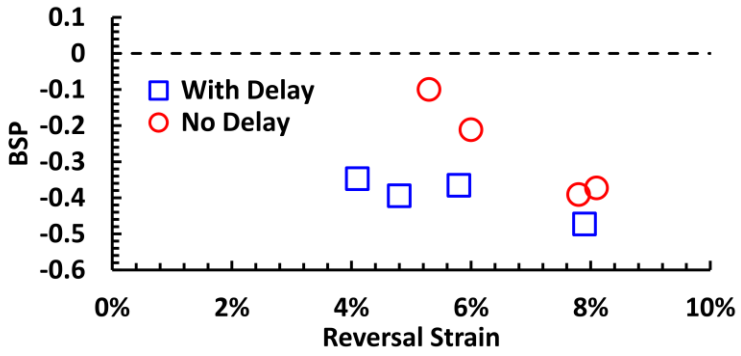

Figure 5.7 BSP as a function of strain level at load reversal for specimens tested with reversal occurring both before and after recovery.

5.4 Results with NC-Cu-10at.%Ta

NC-Cu-10at.%Ta samples, with initial microstructures similar to that observed in chapters 2 and 3, have shown that the deformation mechanism for a stable nanocrystalline material shifts from dislocation mediated plasticity at low strain rates to twin nucleation at high strain rates (see chapter 3). Here, the effect of this change in deformation mechanism on the dynamic Bauschinger effect is investigated by loading a NC-Cu-10at.%Ta round dogbone sample in compression followed by tension using a maraging

steel Kolsky bar with modifications as described above. Results from a dynamic compression followed by tension test are shown in Figure 5.8 along with separately tested dynamic compression and dynamic tension results. Due to limited sample availability, the separate tension test employed a small rectangular dogbone specimen, but due to the difficulty of reversed loading of such a specimen, the compression followed by tension test employed a cylindrical dogbone specimen. As such, flow stress and ductility can only be qualitatively compared.

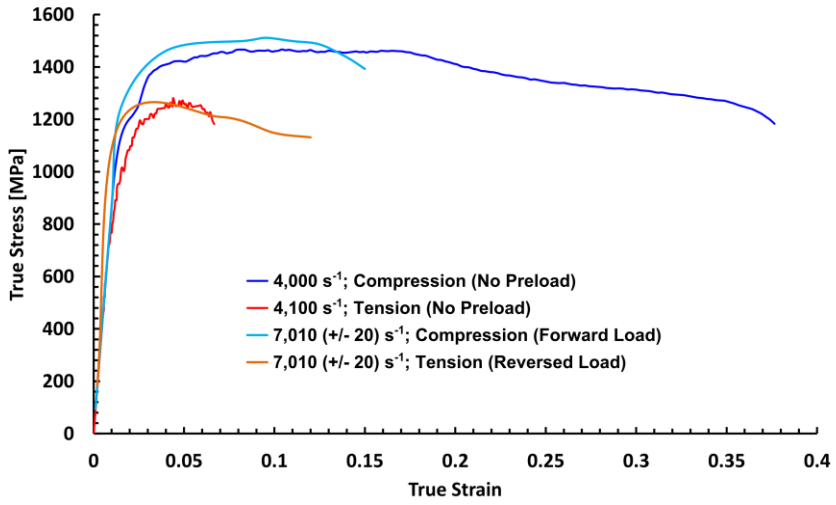

Figure 5.8 Flow stress as a function of strain for NC-Cu-10at.%Ta. Tensile and compressive results are plotted as positive values so that flow stress and ductility can be directly compared.

The tensile and compressive mechanical behavior shows extensive anisotropy, in both flow stress and ductility, inherent in the nanocrystalline material. Prior to testing, the material was shown to be fully dense; however, as the material was processed as powder and consolidated to bulk using ECAE, large Ta particles may exist due to cluster formation during processing leading to an increased number of damage nucleation sites

which would adversely affect the tensile properties of the material without significant effect to the compressive flow stress. When a compressive preload is applied, no noticeable change in flow stress is observed upon load reversal. In fact, if a parameter comparable to the BSP is calculated at a plastic strain of 5%, a comparison of this parameter for the case of dynamic compressive preload to the case of separate dynamic compression and tension tests indicates that little to no effect of preload is observed. The BSP for the preload case is 0.19 while the BSP for the case of separate samples is 0.16. The small difference observed in the BSP may result from adiabatic heating within the dynamically preloaded sample, or detrimental effects, such as stress concentrations, from tensile testing with a rectangular dogbone specimen.

5.5 Conclusions

A novel technique for analyzing the dynamic Bauschinger effect in strain rate sensitive materials has been developed by applying simultaneous tension and compression loading to opposing ends of a Kolsky bar apparatus. The device was successfully employed to analyze the strain rate, strain level, and recovery state dependence of the Bauschinger effect in a 6061-T6 aluminum alloy.

The modified Kolsky bar is shown to be capable of applying reversed uniaxial loads at strain rates up to 7,000 (+/- 20) s^{-1} with a delay between forward and reversed loading of less than 11 ms. This delay was estimated to allow negligible specimen recovery based on an assumption that thermal losses to the sample occur in the form of convective losses to the environment. The modifications are applied separately to a 7075-T6 aluminum

alloy and a C350 maraging steel Kolsky bar in order to analyze low impedance (6061-T6) and high impedance (NC-Cu-10at.%Ta) alloys.

Damage combined with work hardening following tensile load in the 6061-T6 alloy was proposed to cause reversed (compressive) flow stress to increase leading to negative BSP values. This is further supported by the decreasing BSP as forward strain is increased. The Bauschinger effect exhibited strain rate dependence in the 6061-T6 alloy both when the specimen was and was not allowed to recover from adiabatic heating effects; however, the decrease in BSP is lower for the case of no specimen recovery owing to the lower reversed flow stress resulting from the elevated temperature.

Finally, inherent anisotropy in the compressive and tensile flow stress of NC-Cu-10at.%Ta is attributed to the variation in forward and reversed flow stress of the material during dynamic Bauschinger loading. Adiabatic heating may further contribute to the softening of the reversed flow stress, but more testing is required for verification.

6 FUTURE WORK

Extensive mechanical testing of a truly stable nanocrystalline Cu-Ta alloy at high strain rates and high temperatures has been performed; however, the stability of the NC Cu-Ta system makes possible even further investigation into the effects of truly nanocrystalline structure on the mechanical behavior of crystalline materials. Some of the works still lacking in understanding true nanocrystalline behavior are as follows:

1. In chapter 4, Cu-5at.%Ta and Cu-10at.%Ta processed at 700 °C exhibited nanocrystalline structure and similar mechanical properties while Cu-1at.%Ta processed at the same temperature exhibited drastically different mechanical behavior. Further work is needed to determine the specific Ta concentration at which this transition occurs in order to optimize the alloy.
2. Further, the stability of nanocrystalline samples with differing compositions needs to be investigated. Chapter 4 addressed limited mechanical behavior, but no post deformation structural investigation was performed. Also, no investigation into the either the mechanical properties at elevated temperature nor the thermal stability of the Cu-5at.%Ta processed at 700 °C was performed, though this would lead to a better understanding of the effects of Ta concentration on the behavior of nanocrystalline Cu.
3. Comprehensive examination of the dynamic Bauschinger effect in NC-Cu-10at.%Ta is needed in both tension followed by compression and compression followed by tension in order to develop a full understanding of the effects of microstructure change resulting from twin formation during forward loading.

Particularly, the effects of twin formation on the mechanical behavior during reversed loading needs to be further analyzed.

4. Here, the mechanical response under uniaxial load was investigated, but particularly in impact scenarios, materials are prone to shear loading. Therefore, an investigation of the shear response at both low and high strain rates should be performed to analyze the effective strength and ductility under such loading.
5. Using similar techniques to the dynamic load reversal discussed in this work, the combined shear and uniaxial load response should be analyzed. In doing so, the effects of strain rate as well as nanocrystalline grain size on the von Mises and Tresca failure envelopes be probed.

REFERENCES

[1] K.A. Darling, M.A. Tschopp, R.K. Guduru, W.H. Yin, Q. Wei, L.J. Kecskes, Microstructure and mechanical properties of bulk nanostructured Cu–Ta alloys consolidated by equal channel angular extrusion, Acta Mater. 76 (2014) 168–185. doi:10.1016/j.actamat.2014.04.074.

[2] G.E. Dieter, Mechanical Metallurgy, 3rd ed., McGraw-Hill, 1986.

[3] L. Lu, M.L. Sui, K. Lu, Superplastic Extensibility of Nanocrystalline Copper at Room Temperature, Science. 287 (2000) 1463–1466. doi:10.1126/science.287.5457.1463.

[4] S.X. McFadden, R.S. Mishra, R.Z. Valiev, A.P. Zhilyaev, A.K. Mukherjee, Low-temperature superplasticity in nanostructured nickel and metal alloys, Nature. 398 (1999) 684–686. doi:10.1038/19486.

[5] U. Klement, U. Erb, A.M. El-Sherik, K.T. Aust, Thermal stability of nanocrystalline Ni, Mater. Sci. Eng. A. 203 (1995) 177–186. doi:10.1016/0921-5093(95)09864-X.

[6] R.A. Andrievski, Review of thermal stability of nanomaterials, J. Mater. Sci. 49 (2014) 1449–1460. doi:10.1007/s10853-013-7836-1.

[7] R.A. Andrievski, Review Stability of nanostructured materials, J. Mater. Sci. 38 (2003) 1367–1375. doi:10.1023/A:1022988706296.

[8] C.C. Koch, Structural nanocrystalline materials: an overview, J. Mater. Sci. 42 (2007) 1403–1414. doi:10.1007/s10853-006-0609-3.

[9] C.C. Koch, R.O. Scattergood, M. Saber, H. Kotan, High temperature stabilization of nanocrystalline grain size: Thermodynamic versus kinetic strategies, J. Mater. Res. (2013). doi:10.1557/jmr.2012.429.

[10] H.A.P. Ii, B.L. Boyce, A Review of Fatigue Behavior in Nanocrystalline Metals, Exp. Mech. 50 (2009) 5–23. doi:10.1007/s11340-009-9301-2.

[11] D. Sagapuram, Z. Wang, C. Saldana, Thermal stability of nanotwinned and nanocrystalline microstructures produced by cryogenic shear deformation, Philos. Mag. 94 (2014) 3413–3430. doi:10.1080/14786435.2014.958590.

[12] K.A. Darling, E.L. Huskins, B.E. Schuster, Q. Wei, L.J. Kecskes, Mechanical properties of a high strength Cu–Ta composite at elevated temperature, Mater. Sci. Eng. A. 638 (2015) 322–328. doi:10.1016/j.msea.2015.04.069.

[13] M. Rajagopalan, K. Darling, S. Turnage, R.K. Koju, B. Hornbuckle, Y. Mishin, K.N. Solanki, Microstructural evolution in a nanocrystalline Cu-Ta alloy: A combined in-situ TEM and atomistic study, Mater. Des. 113 (2017) 178–185. doi:10.1016/j.matdes.2016.10.020.

[14] J.L. Jordan, C.R. Siviour, G. Sunny, C. Bramlette, J.E. Spowart, Strain rate-dependant mechanical properties of OFHC copper, J. Mater. Sci. 48 (2013) 7134–7141. doi:10.1007/s10853-013-7529-9.

[15] J.W. House, J.C. Lewis, P.P. Gillis, L.L. Wilson, Estimation of flow stress under high rate plastic deformation, Int. J. Impact Eng. 16 (1995) 189–200. doi:10.1016/0734-743X(94)00042-U.

[16] M.A. Meyers, Dynamic Behavior of Materials, John Wiley and Sons Inc., New York, 1994.

[17] M. Dao, L. Lu, Y.F. Shen, S. Suresh, Strength, strain-rate sensitivity and ductility of copper with nanoscale twins, Acta Mater. 54 (2006) 5421–5432. doi:10.1016/j.actamat.2006.06.062.

[18] F. Dalla Torre, H. Van Swygenhoven, M. Victoria, Nanocrystalline electrodeposited Ni: microstructure and tensile properties, Acta Mater. 50 (2002) 3957–3970. doi:10.1016/S1359-6454(02)00198-2.

[19] G. Regazzoni, U.F. Kocks, P.S. Follansbee, Dislocation kinetics at high strain rates, Acta Metall. 35 (1987) 2865–2875. doi:10.1016/0001-6160(87)90285-9.

[20] E. Nadgornyi, Dislocation dynamics and mechanical properties of crystals, Prog. Mater. Sci. 31 (1988) 1–530. doi:10.1016/0079-6425(88)90005-9.

[21] G.P. Srivastava, The physics of phonons, CRC Press, 1990.

[22] L. Xiong, J. Rigelesaiyin, X. Chen, S. Xu, D.L. McDowell, Y. Chen, Coarse-grained elastodynamics of fast moving dislocations, Acta Mater. 104 (2016) 143–155.

[23] L. Davison, Fundamentals of Shock Wave Propagation in Solids, Springer, 2008. http://www.springer.com/us/book/9783540745686 (accessed April 3, 2017).

[24] D. Rittel, A. Bhattacharyya, B. Poon, J. Zhao, G. Ravichandran, Thermomechanical characterization of pure polycrystalline tantalum, Mater. Sci. Eng. A. 447 (2007) 65–70. doi:10.1016/j.msea.2006.10.064.

[25] A.V. Yanilkin, V.S. Krasnikov, A.Y. Kuksin, A.E. Mayer, Dynamics and kinetics of dislocations in Al and Al–Cu alloy under dynamic loading, Int. J. Plast. 55 (2014) 94–107. doi:10.1016/j.ijplas.2013.09.008.

[26] B.A. Gama, S.L. Lopatnikov, J. Gillespie John W., Hopkinson bar experimental technique: A critical review, Appl. Mech. Rev. 57 (2004) 223–250. doi:10.1115/1.1704626.

[27] G.T. Gray III, Mechanical Testing and Evaluation: Classic Split-Hopkinson Pressure Bar Testing, in: ASM Handb., ASM International, 2000: pp. 462–476.

[28] R. Kapoor, S. Nemat-Nasser, Determination of temperature rise during high strain rate deformation, Mech. Mater. 27 (1998) 1–12. doi:10.1016/S0167-6636(97)00036-7.

[29] C. Bacon, J. Carlsson, J.L. Lataillade, EVALUATION OF FORCE AND PARTICLE VELOCITY AT THE HEATED END OF A ROD SUBJECTED TO IMPACT LOADING, J. Phys. IV. 01 (1991) C3-395-C3-402. doi:10.1051/jp4:1991356.

[30] G. Taylor, The Use of Flat-Ended Projectiles for Determining Dynamic Yield Stress. I. Theoretical Considerations, Proc. R. Soc. Lond. Math. Phys. Eng. Sci. 194 (1948) 289–299. doi:10.1098/rspa.1948.0081.

[31] S.E. Jones, P.P. Gillis, J.C. Foster, On the equation of motion of the undeformed section of a Taylor impact specimen, J. Appl. Phys. 61 (1987) 499–502. doi:10.1063/1.338249.

[32] O.D. Sherby, J. Wadsworth, Superplasticity—Recent advances and future directions, Prog. Mater. Sci. 33 (1989) 169–221. doi:10.1016/0079-6425(89)90004-2.

[33] V. Yamakov, D. Wolf, S.R. Phillpot, A.K. Mukherjee, H. Gleiter, Deformation-mechanism map for nanocrystalline metals by molecular-dynamics simulation, Nat. Mater. 3 (2004) 43–47. doi:10.1038/nmat1035.

[34] H. Gleiter, Nanostructured materials: basic concepts and microstructure, Acta Mater. 48 (2000) 1–29. doi:10.1016/S1359-6454(99)00285-2.

[35] K.A. Darling, M.A. Tschopp, R.K. Guduru, W.H. Yin, Q. Wei, L.J. Kecskes, Microstructure and mechanical properties of bulk nanostructured Cu–Ta alloys consolidated by equal channel angular extrusion, Acta Mater. 76 (2014) 168–185. doi:10.1016/j.actamat.2014.04.074.

[36] K.A. Darling, M. Rajagopalan, M. Komarasamy, M.A. Bhatia, B.C. Hornbuckle, R.S. Mishra, K.N. Solanki, Extreme creep resistance in a microstructurally stable nanocrystalline alloy, Nature. 537 (2016) 378–381. doi:10.1038/nature19313.

[37] V.M. Segal, Materials processing by simple shear, Mater. Sci. Eng. A. 197 (1995) 157–164. doi:10.1016/0921-5093(95)09705-8.

[38] M. Furukawa, Z. Horita, M. Nemoto, T.G. Langdon, Review: Processing of metals by equal-channel angular pressing, J. Mater. Sci. 36 (2001) 2835–2843. doi:10.1023/A:1017932417043.

[39] Y.T. Zhu, T.C. Lowe, Observations and issues on mechanisms of grain refinement during ECAP process, Mater. Sci. Eng. A. 291 (2000) 46–53. doi:10.1016/S0921-5093(00)00978-3.

[40] B.C. Hornbuckle, T. Rojhirunsakool, M. Rajagopalan, T. Alam, G.P.P. Pun, R. Banerjee, K.N. Solanki, Y. Mishin, L.J. Kecskes, K.A. Darling, Effect of Ta Solute Concentration on the Microstructural Evolution in Immiscible Cu-Ta Alloys, JOM. 67 (2015) 2802–2809. doi:10.1007/s11837-015-1643-x.

[41] M. Bhatia, M. Rajagopalan, K. Darling, M. Tschopp, K. Solanki, The role of Ta on twinnability in nanocrystalline Cu–Ta alloys, Mater. Res. Lett. 5 (2017) 48–54.

[42] W.F. Gale, T.C. Totemeier, eds., Front Matter, in: Smithells Met. Ref. Book Eighth Ed., Butterworth-Heinemann, Oxford, 2004: p. iii. doi:10.1016/B978-0-7506-7509-3.50046-4.

[43] J. Schiøtz, K.W. Jacobsen, A Maximum in the Strength of Nanocrystalline Copper, Science. 301 (2003) 1357–1359. doi:10.1126/science.1086636.

[44] H. Van Swygenhoven, A. Caro, D. Farkas, A molecular dynamics study of polycrystalline fcc metals at the nanoscale: grain boundary structure and its influence on plastic deformation, Mater. Sci. Eng. A. 309–310 (2001) 440–444. doi:10.1016/S0921-5093(00)01794-9.

[45] H.V. Swygenhoven, A. Caro, Plastic behavior of nanophase Ni: A molecular dynamics computer simulation, Appl. Phys. Lett. 71 (1997) 1652–1654. doi:10.1063/1.119785.

[46] H. Van Swygenhoven, P.M. Derlet, A. Hasnaoui, Atomic mechanism for dislocation emission from nanosized grain boundaries, Phys. Rev. B. 66 (2002) 024101. doi:10.1103/PhysRevB.66.024101.

[47] J. Hirth, J. Lothe, Theory of Dislocations, 780 pp, McGraw-Hill, New York, 1968.

[48] T. Chookajorn, H.A. Murdoch, C.A. Schuh, Design of Stable Nanocrystalline Alloys, Science. 337 (2012) 951–954. doi:10.1126/science.1224737.

[49] M.A. Meyers, A. Mishra, D.J. Benson, Mechanical properties of nanocrystalline materials, Prog. Mater. Sci. 51 (2006) 427–556. doi:10.1016/j.pmatsci.2005.08.003.

[50] W.F. Greenman, T.V. Jr, D.S. Wood, Dislocation Mobility in Copper, J. Appl. Phys. 38 (1967) 3595–3603. doi:10.1063/1.1710178.

[51] A. Kumar, R.G. Kumble, Viscous Drag on Dislocations at High Strain Rates in Copper, J. Appl. Phys. 40 (1969) 3475–3480. doi:10.1063/1.1658222.

[52] D. Rittel, A. Bhattacharyya, B. Poon, J. Zhao, G. Ravichandran, Thermomechanical characterization of pure polycrystalline tantalum, Mater. Sci. Eng. A. 447 (2007) 65–70.

[53] Q. Wei, B.E. Schuster, S.N. Mathaudhu, K.T. Hartwig, L.J. Kecskes, R.J. Dowding, K.T. Ramesh, Dynamic behaviors of body-centered cubic metals with ultrafine grained and nanocrystalline microstructures, Mater. Sci. Eng. A. 493 (2008) 58–64. doi:10.1016/j.msea.2007.05.126.

[54] D. Jia, Y.M. Wang, K.T. Ramesh, E. Ma, Y.T. Zhu, R.Z. Valiev, Deformation behavior and plastic instabilities of ultrafine-grained titanium, Appl. Phys. Lett. 79 (2001) 611–613. doi:10.1063/1.1384000.

[55] H.-S. Park, R.E. Rudd, R.M. Cavallo, N.R. Barton, A. Arsenlis, J.L. Belof, K.J.M. Blobaum, B.S. El-dasher, J.N. Florando, C.M. Huntington, B.R. Maddox, M.J. May, C. Plechaty, S.T. Prisbrey, B.A. Remington, R.J. Wallace, C.E. Wehrenberg, M.J. Wilson, A.J. Comley, E. Giraldez, A. Nikroo, M. Farrell, G. Randall, G.T. Gray, Grain-Size-Independent Plastic Flow at Ultrahigh Pressures and Strain Rates, Phys. Rev. Lett. 114 (2015) 065502. doi:10.1103/PhysRevLett.114.065502.

[56] S. Yip, Nanocrystals: The strongest size, Nature. 391 (1998) 532–533. doi:10.1038/35254.

[57] J. Hu, Y.N. Shi, X. Sauvage, G. Sha, K. Lu, Grain boundary stability governs hardening and softening in extremely fine nanograined metals, Science. 355 (2017) 1292–1296. doi:10.1126/science.aal5166.

[58] D. Jia, K.T. Ramesh, E. Ma, Effects of nanocrystalline and ultrafine grain sizes on constitutive behavior and shear bands in iron, Acta Mater. 51 (2003) 3495–3509. doi:10.1016/S1359-6454(03)00169-1.

[59] D. Jia, K.T. Ramesh, E. Ma, L. Lu, K. Lu, Compressive behavior of an electrodeposited nanostructured copper at quasistatic and high strain rates, Scr. Mater. 45 (2001) 613–620. doi:10.1016/S1359-6462(01)01071-5.

[60] B. Banerjee, TAYLOR IMPACT TESTS: DETAILED REPORT, University of Utah, Salt Lake City, Utah, 2005. http://www.sci.utah.edu/publications/Ban2005a/Banerjee_CSAFE-Report2005.pdf.

[61] G. Johnson R., W.H. Cook, A constitutive model and data for metals subjected to large strains, high strain rates and high temperatures., Proc. 7th Int. Symp. Ballist. 21 (1983) 541–547.

[62] R. Peierls, The size of a dislocation, Proc. Phys. Soc. 52 (1940) 34. doi:10.1088/0959-5309/52/1/305.

[63] P.S. Follansbee, U.F. Kocks, A constitutive description of the deformation of copper based on the use of the mechanical threshold stress as an internal state variable, Acta Metall. 36 (1988) 81–93. doi:10.1016/0001-6160(88)90030-2.

[64] S. Nemat-Nasser, Y. Li, Flow stress of f.c.c. polycrystals with application to OFHC Cu, Acta Mater. 46 (1998) 565–577. doi:10.1016/S1359-6454(97)00230-9.

[65] F.J. Zerilli, R.W. Armstrong, The effect of dislocation drag on the stress-strain behavior of F.C.C. metals, Acta Metall. Mater. 40 (1992) 1803–1808. doi:10.1016/0956-7151(92)90166-C.

[66] D.A. Gorham, The effect of specimen dimensions on high strain rate compression measurements of copper, J. Phys. Appl. Phys. 24 (1991) 1489. doi:10.1088/0022-3727/24/8/041.

[67] P.S. Follansbee, G.T. Gray, Dynamic deformation of shock prestrained copper, Mater. Sci. Eng. A. 138 (1991) 23–31. doi:10.1016/0921-5093(91)90673-B.

[68] D.L. McDowell, Internal State Variable Theory, in: S. Yip (Ed.), Handb. Mater. Model., Springer Netherlands, 2005: pp. 1151–1169. doi:10.1007/978-1-4020-3286-8_58.

[69] T.J. Rupert, D.S. Gianola, Y. Gan, K.J. Hemker, Experimental Observations of Stress-Driven Grain Boundary Migration, Science. 326 (2009) 1686–1690. doi:10.1126/science.1178226.

[70] D.S. Gianola, S. Van Petegem, M. Legros, S. Brandstetter, H. Van Swygenhoven, K.J. Hemker, Stress-assisted discontinuous grain growth and its effect on the

deformation behavior of nanocrystalline aluminum thin films, Acta Mater. 54 (2006) 2253–2263. doi:10.1016/j.actamat.2006.01.023.

[71] W. Chen, F. Lu, M. Cheng, Tension and compression tests of two polymers under quasi-static and dynamic loading, Polym. Test. 21 (2002) 113–121. doi:10.1016/S0142-9418(01)00055-1.

[72] J. Bauschinger, Changes of the elastic limit and the modulus of elasticity on various metals, Zivilingenieur. 27 (1881) 289–348.

[73] J.D.H. Paul, R. Hoppe, F. Appel, On the Bauschinger effect in TiAl alloys, Acta Mater. 104 (2016) 101–108. doi:10.1016/j.actamat.2015.10.036.

[74] J. Rajagopalan, C. Rentenberger, H. Peter Karnthaler, G. Dehm, M.T.A. Saif, In situ TEM study of microplasticity and Bauschinger effect in nanocrystalline metals, Acta Mater. 58 (2010) 4772–4782. doi:10.1016/j.actamat.2010.05.013.

[75] M. Haouaoui, I. Karaman, H.J. Maier, Flow stress anisotropy and Bauschinger effect in ultrafine grained copper, Acta Mater. 54 (2006) 5477–5488. doi:10.1016/j.actamat.2006.07.022.

[76] J.B. Jordon, M.F. Horstemeyer, K. Solanki, Y. Xue, Damage and stress state influence on the Bauschinger effect in aluminum alloys, Mech. Mater. 39 (2007) 920–931. doi:10.1016/j.mechmat.2007.03.004.

[77] G.E. Nevill Jr., C.D. Myers, Strain rate effects during reversed loading, J. Mech. Phys. Solids. 16 (1968) 187–194. doi:10.1016/0022-5096(68)90027-6.

[78] J. Peirs, P. Verleysen, J. Degrieck, Study of the dynamic Bauschinger effect in Ti6Al4V by torsion experiments, EPJ Web Conf. 26 (2012) 01023. doi:10.1051/epjconf/20122601023.

[79] S. Nemat-Nasser, J.B. Isaacs, J.E. Starrett, Hopkinson Techniques for Dynamic Recovery Experiments, Proc. R. Soc. Lond. Ser. Math. Phys. Sci. 435 (1991) 371–391. doi:10.1098/rspa.1991.0150.

[80] B. Song, W. Chen, Loading and unloading split hopkinson pressure bar pulse-shaping techniques for dynamic hysteretic loops, Exp. Mech. 44 (2004) 622–627. doi:10.1007/BF02428252.

[81] G.M. Owolabi, A.G. Odeshi, M.N.K. Singh, M.N. Bassim, Dynamic shear band formation in Aluminum 6061-T6 and Aluminum 6061-T6/Al2O3 composites, Mater. Sci. Eng. A. 457 (2007) 114–119. doi:10.1016/j.msea.2006.12.034.